

## Chapter 4

# Results and Analysis: Characterization of Dielectric Barrier Discharge

The results are presented in two chapters; the present chapter on the electrical characteristics of the DBD and its physical appearance as well as its optical emission spectra while the next chapter focuses on the bacteria sterilization/inactivation application aspect.

### 4.1 Electrical Characteristics of DBD

The electrical characteristics of the DBD operated with glass and alumina are presented. The parameters monitored are the discharge voltage and current while the variables are the air-gap width, frequency and amplitude of the applied voltage.

#### 4.1.1 Frequency consideration

##### 4.1.1.1 Electrical resonance condition for glass dielectric barrier

The resonant condition of the DBD electrical circuit is sought so that maximum sinusoidal discharge voltage may be obtained and efficiency optimized. The results obtained with glass as the dielectric barrier is presented here. The peak-to-peak DBD voltage (a capacitive voltage) at resonance condition depends on the drive voltage (controlled by the drain voltage,  $V_{DD}$ ) from the MOSFET. Figure 4.1 shows that DBD voltage increases linearly with  $V_{DD}$  initially until the field inside the gap exceeds the reduced Paschen field and breakdown is induced. This point is indicated by the dashed

arrow at which the curve begins to saturate and the peak DBD voltage here is taken to be the breakdown voltage,  $V_{bd}$ . Diffuse-like or filamentary plasma is formed between the gap after breakdown. The DBD voltage increases slower after the breakdown due to charge deposition on the dielectric surface and building up of local electric field which reduces the effective applied field.

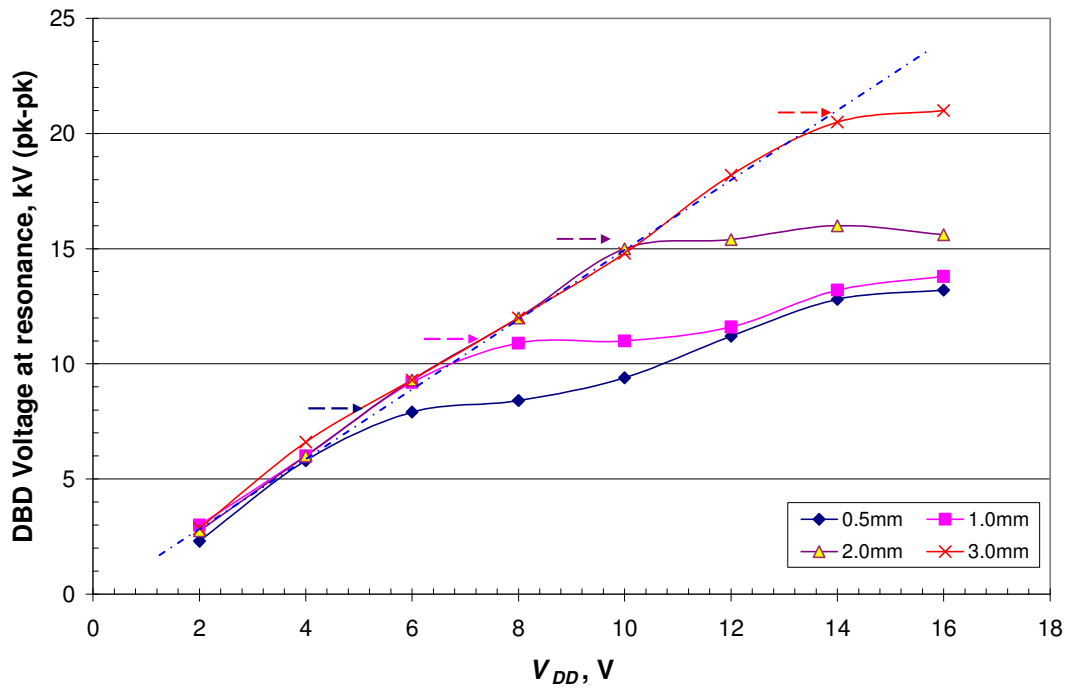


**Figure 4.1:** DBD voltage (pk-pk) versus  $V_{DD}$  of MOSFET for four air-gap sizes with glass dielectric. The dashed arrows indicate DBD voltage when “saturation” begins to occur.

The breakdown voltage  $V_{bd}$  is found to depend on gap distance as given in Table 4.1. In assuming uniform electric field in the glass and air regions, the corresponding electric field in the air-gap  $E_{air-gap}$  is computed from:

$$E_{air-gap} = \frac{V_{bd}}{d_{air-gap} + \frac{\epsilon_0}{\epsilon_g} d_g}, \quad (4.1)$$

where  $d_{\text{air-gap}}$  and  $d_g$  are the width of the air gap and glass dielectric sheet respectively, and  $\epsilon_0$  and  $\epsilon_g$  the permittivity in air and glass dielectric sheet respectively. The computed  $E_{\text{air-gap}}$  is close to the dielectric strength in air, i.e., 3.4kV/mm (Pashaia *et al.*, 1999), except for 0.5mm and 1mm gaps. On closer scrutiny of the curves in Figure 4.1, point at which saturation begins is less clear for the narrow gaps, hence,  $V_{bd}$  used for computing  $E_{\text{air-gap}}$  is probably over-estimated. However,  $V_{bd}$  rises as air-gap width increases which is consistent with the behaviour to the right hand side of the Paschen minimum.

**Table 4.1:** Dependence of DBD voltage on gap width for plasma ignition with glass dielectric barrier at atmospheric pressure.

Gap width	Breakdown voltage, $V_{bd}$	Corresponding electric field in the air gap at breakdown computed from Eq. (4.1)	Breakdown voltage computed from Eq. (2b)
0.5mm	~4kV	5.2kV/mm	2.85kV
1.0mm	~5.5kV	4.3kV/mm	4.35kV
2.0mm	~7.8kV	3.4kV/mm	7.35kV
3.0mm	~10.5kV	3.2kV/mm	10.35kV

The resonant frequency (sinusoidal waveform) at which highest peak-to-peak sinusoidal DBD voltage is found for different air-gap distances and shown in Figure 4.2. The increase of the resonant frequency  $f_{res}$  with air-gap distance is expected since the capacitance across the DBD electrodes decreases with increased gap distance (Table 3.1) and  $f_{res} = 1/(2\pi\sqrt{LC})$ ,  $L$  is the resonance (series) inductance of the ignition coil transformer which is assumed constant. This resonance series inductance is deduced by noting the resonance frequency when a known capacitance (Murata ceramic capacitors, each 440pF) is connected to output of the power supply (across the secondary coil of the step-up transformer). The estimated value of  $L$  is (6.8±0.2)H.

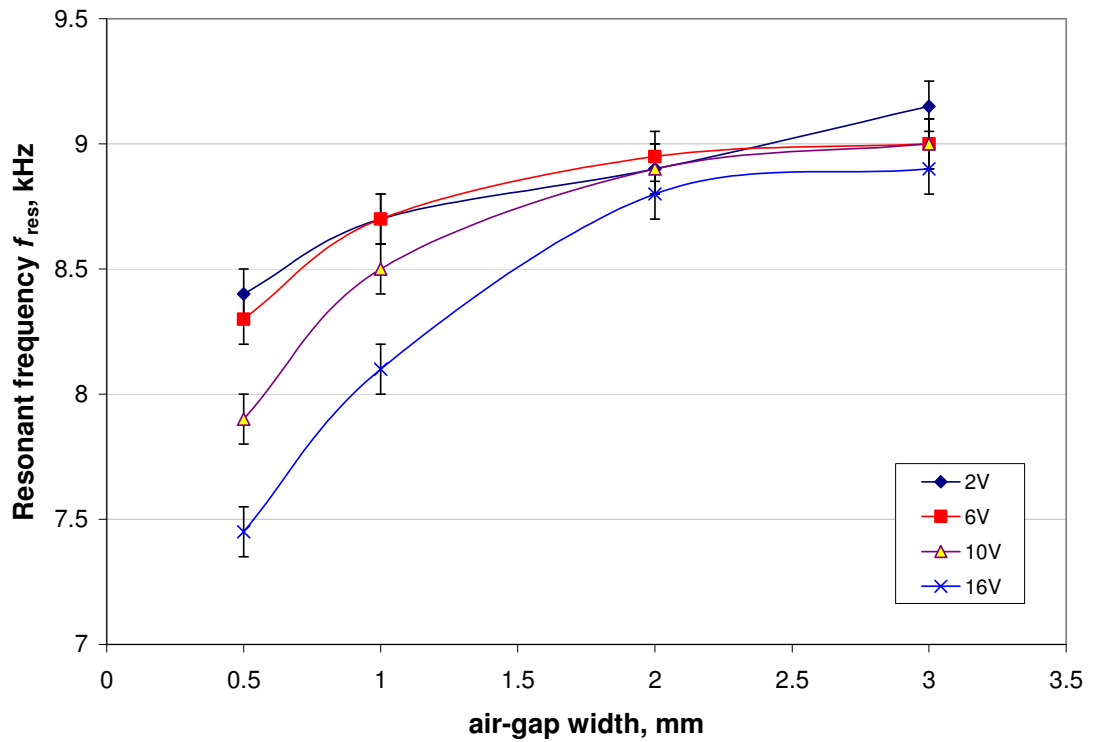


**Figure 4.2:** Resonance frequency of DBD dependence on air-gap size (Glass dielectric) at  $V_{DD} = 2V, 6V, 10V$  and  $16V$ .

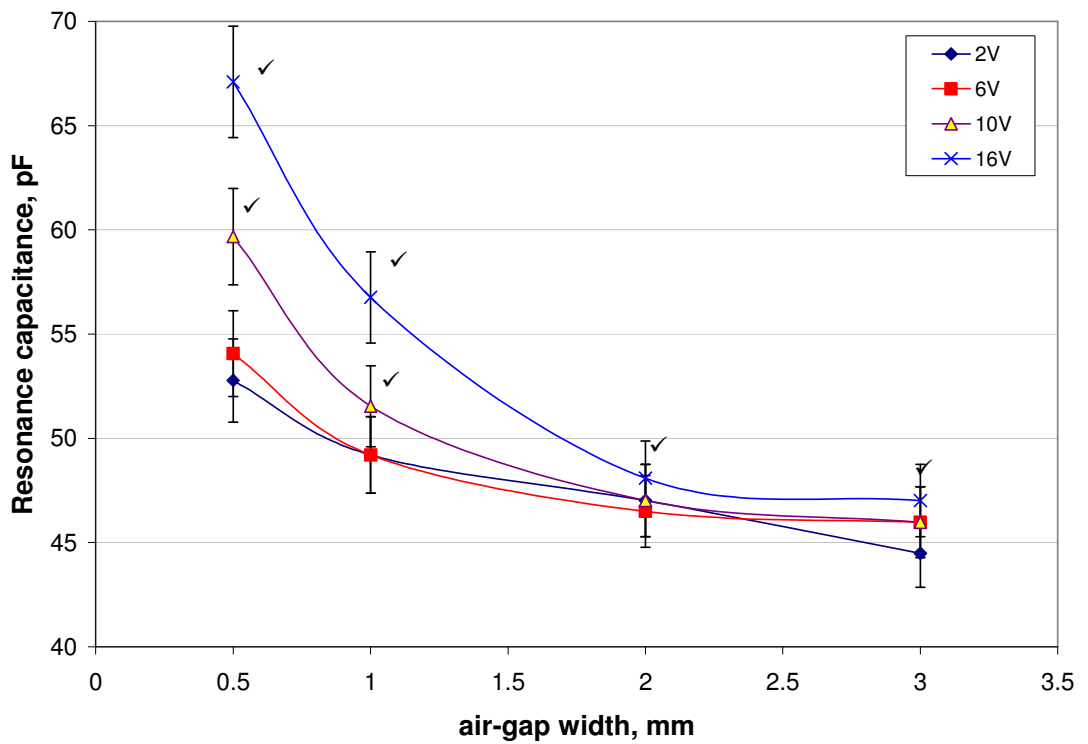


**Figure 4.3:** Capacitance of DBD at resonance deduced for different air-gap size (Glass dielectric) at  $V_{DD} = 2V, 6V, 10V$  and  $16V$ . The 'tick' indicates breakdown of gap has occurred.

The capacitance of the DBD at resonance is deduced and shown in Figure 4.3. At low  $V_{DD}$ , e.g. 2V and 6V, the deduced capacitance is about (54-46) pF, approximately 40pF higher than those calculated in Table 3.1. Though there is no visible glow or filaments, there is some ionization in the air-gap and charge accumulation on the dielectric surface. This tends to increase the capacity of the parallel-plate arrangement to store charges. It is as if the air-gap has reduced or vanished and the other electrode is brought into contact with the dielectric surface, thereby, the capacitance is close to that with only the glass dielectric layer (estimated to be 38pF). In addition, there is contribution of stray capacitances from the H.V. probe connected and connection wires. When the plasma is visible and the gap becomes greatly conducting, e.g. at  $V_{DD} = 16V$  and gap of 0.5mm where the filaments are profusely formed, the estimated resonance capacitance is distinctly raised. The glass dielectric sheet used is bought from a normal picture framing shop, hence, its surface finish is of low quality. Charges can get into the micro cavities and therefore, further reducing the thickness of the sheet and increases the capacitance.

#### 4.1.1.2 Discharge voltage measured for various air-gap sizes with glass dielectric barrier

For the frequency range of ~100Hz to 12kHz, the DBD discharge voltage exhibits sinusoidal waveform from 6.5kHz onwards; and distinctive “unipolar” pulses at frequency less than 2.5kHz. The peak to peak discharge voltage is recorded at varying discharge frequency for fixed driving power defined by  $V_{DD}$ . The experiment is repeated for three different air-gap sizes, i.e. 0.5mm, 1.5mm, and 3.0mm.

## 0.5mm air-gap

The study is carried out with glass dielectric at various MOSFET driving voltage  $V_{DD} = 2V, 8V, \text{ and } 14V$  for this air-gap size and discharge voltage characteristics are compared in Figure 4.4. “Unipolar” pulses is obtained for driving frequency below 2.5kHz, and sinusoidal voltage discharge is obtained for driving frequency above 6kHz, resonance frequency (at which sinusoidal voltage waveform peaks) occurs at (7.5-8.5)kHz. Resonant frequency is higher for lower  $V_{DD}$  (when there is no visible microdischarge). Microdischarges (breakdown) start to form at driving voltages above 8.5kV. The magnitude of the “unipolar” pulses rises when frequency is lowered towards  $10^2\text{Hz}$ . The discharge voltage generally increases with larger MOSFET drive voltage,  $V_{DD}$ .

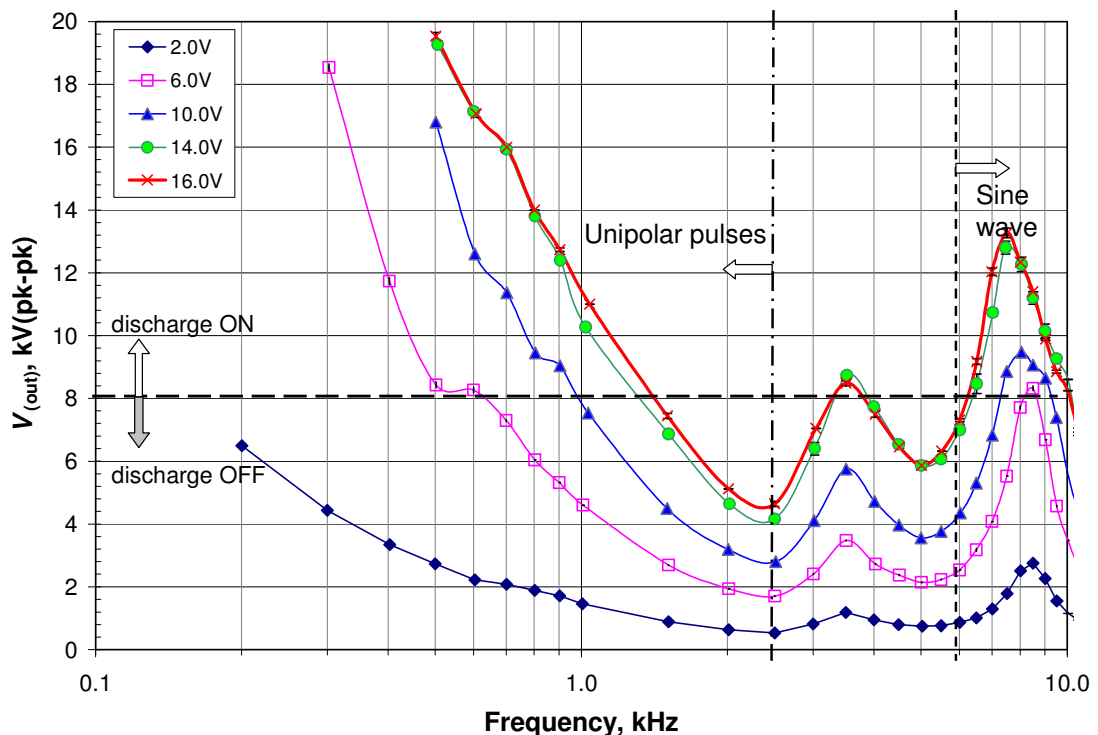


**Figure 4.4:** Discharge voltage (peak to peak) versus frequency for 0.5mm air-gap with glass dielectric (at  $V_{DD} = 2.0V, 6.0V, 10.0V, 14.0V, \text{ and } 16.0V$ ).

### 1.5mm air-gap

For air-gap of 1.5mm, “unipolar” pulsed and sinusoidal wave discharges are obtained in similar frequency ranges (Figure 4.5). Breakdown in the air-gap is induced at higher voltage,  $\geq 11\text{kV}$  and resonance frequency is slightly higher at 8.5 kHz. Figure 4.5 also compares the discharge voltage (peak-to-peak) for various driving powers of the MOSFET drain bias at  $V_{DD} = 2\text{V}$ , 6V, 10V, 14V and 16V at 1.5mm air-gap. Similar to the case of 0.5mm air-gap, the discharge voltage profile shifts to higher value across the frequency as  $V_{DD}$  is increased.

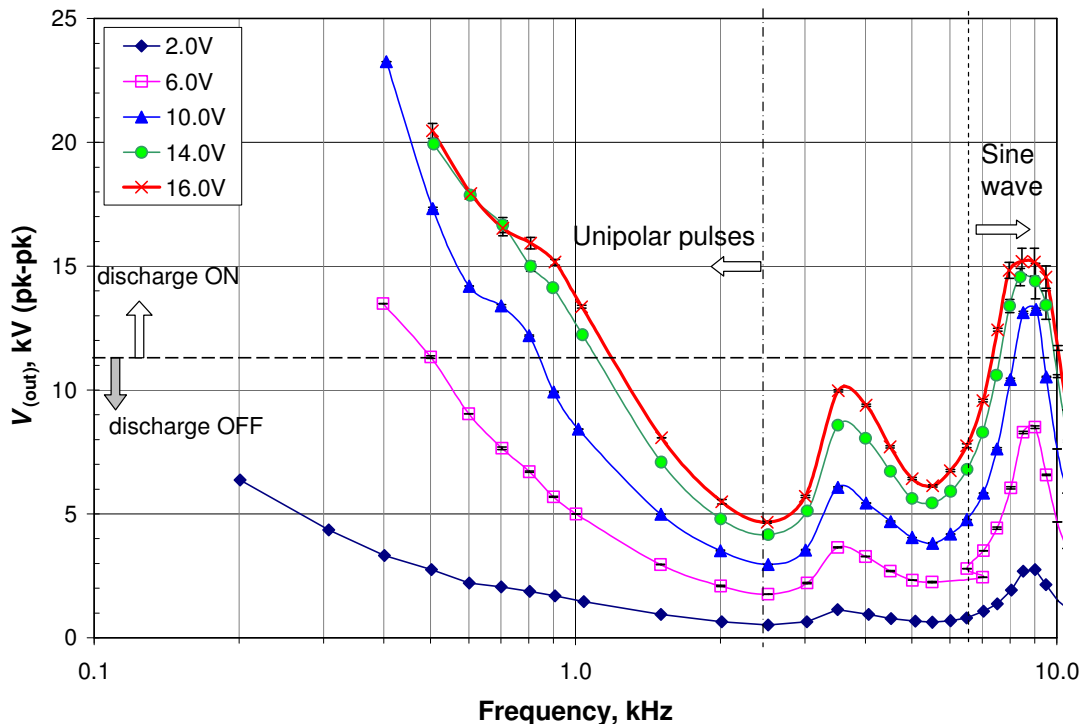


**Figure 4.5:** Discharge voltage (peak to peak) versus frequency for 1.5mm air-gap with glass dielectric (at  $V_{DD} = 2.0\text{V}$ , 6.0V, 10.0V, 14.0V, and 16.0V).

### 3.0mm air-gap

For air-gap of 3.0mm, “unipolar” pulsed discharge is similarly obtained at driving frequency below 2.5kHz, and sinusoidal wave discharge is obtained for driving

frequency above 6.5 kHz. Resonance frequency occurs at yet higher value of 9kHz as seen from Figure 4.6. For this case, there is no distinct breakdown across the gap as driving voltage above 21kV is required. Figure 4.6 also compares the discharge voltage variation with frequency for  $V_{DD} = 2V, 6V, 10V, 14V,$  and  $16V,$  and similar trends are observed.

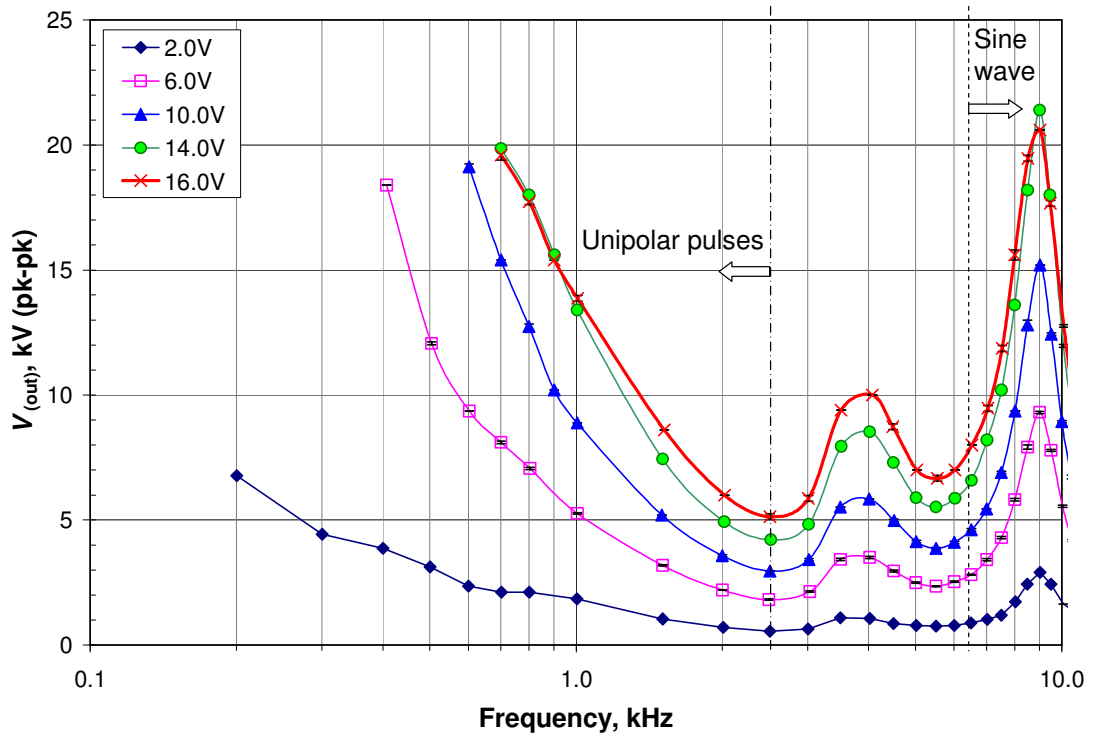


**Figure 4.6:** Discharge voltage (peak to peak) versus frequency for 3.0mm air-gap with glass dielectric (at  $V_{DD} = 2.0V, 6.0V, 10.0V, 14.0V,$  and  $16.0V$ ).

#### 4.1.1.3 Electrical resonance condition for alumina dielectric barrier

The experiments are repeated for comparison with the alumina dielectric. The DBD voltage at resonance increases with the driving power of the MOSFET (controlled by its drain bias voltage  $V_{DD}$ ) for air-gap width ranging from 0.5mm to 3.0mm (Figure 4.7). This trend is similar to that observed earlier in glass DBD. Breakdown of the air-



gap is identified by the initial presence of filaments or diffuse glow in the gap and Table 4.2 lists the estimated breakdown voltage for various gap widths. The values are quite close to that for glass DBD. Though the dielectric strength for alumina of 97.5% purity is 10-35kV/mm (*Goodfellow Cambridge Ltd.*) corresponding to 1-2 times higher than that for glass, its thickness has been reduced by half. Thus, the ‘breakdown field’ for the gap is almost the same in both cases.

**Table 4.2:** Dependence of DBD voltage on air-gap width for plasma ignition with alumina dielectric barrier in atmospheric pressure.

Gap width	Breakdown voltage, $V_{bd}$	Corresponding electric field in the air gap at breakdown computed from Eq. (4.1)	Breakdown voltage computed from Eq. (2a)
0.5mm	~4kV	6.5kV/mm	2.85kV
1.5mm	~6kV	3.7kV/mm	5.85kV
3.0mm	~10.3kV	3.3kV/mm	10.35kV

Trends similar to those for glass dielectric are observed in the resonant frequency (Figure 4.8) and capacitance of the DBD at resonance (Figure 4.9) for the alumina barrier. The capacitance of the DBD is increased by about (35-43)pF compared to the calculated values from the dimensions of the electrodes and dielectric layers given in Table 3.2 when there is no visible plasma in the air-gap. When profuse filaments occur within the gap, the estimated capacitance is greatly enhanced (e.g. at  $V_{DD} = 16V$ , gap width = 0.5mm,  $C_{DBD} = 76pF$ ). However, these values are still lower than the capacitance calculated for only the alumina layer (90pF). This is probably due to the higher quality of surface finish of alumina sheet as compared to the glass sheet discussed in Section 4.1.1.1.

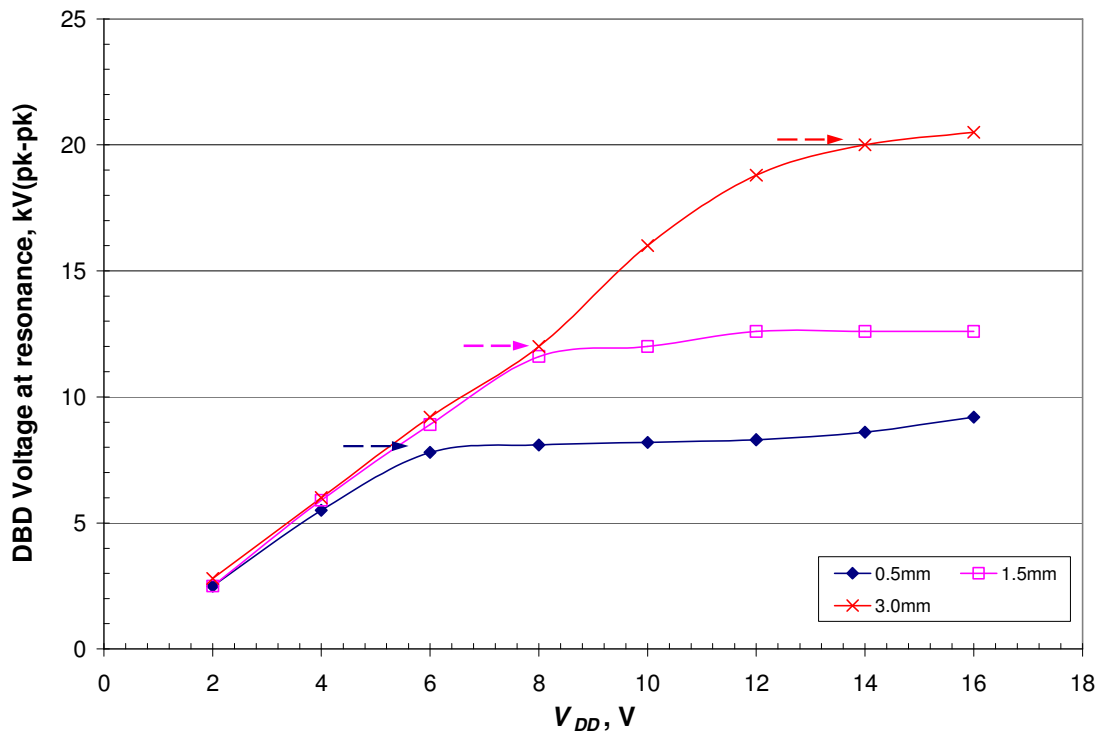


**Figure 4.7:** DBD voltage (pk-pk) versus  $V_{DD}$  of MOSFET for four air-gap sizes with alumina dielectric. The dashed arrows indicate DBD voltage when the curve tends to saturate and the plasma is ‘ON’.

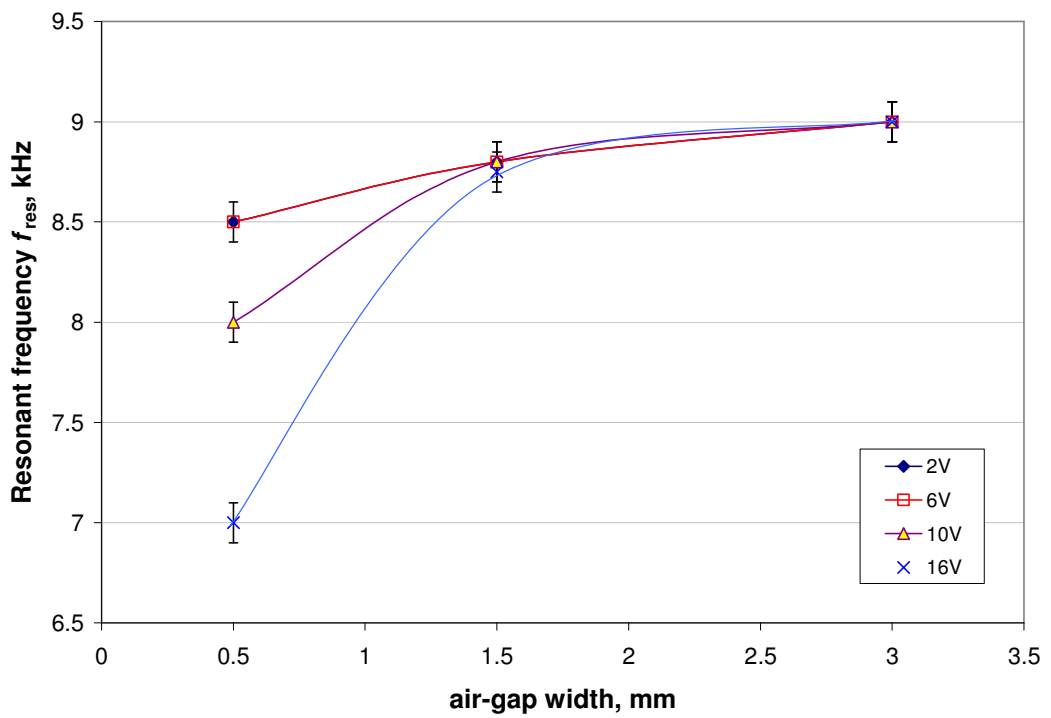


**Figure 4.8:** Resonance frequency range of DBD for various air-gap sizes (Alumina dielectric).

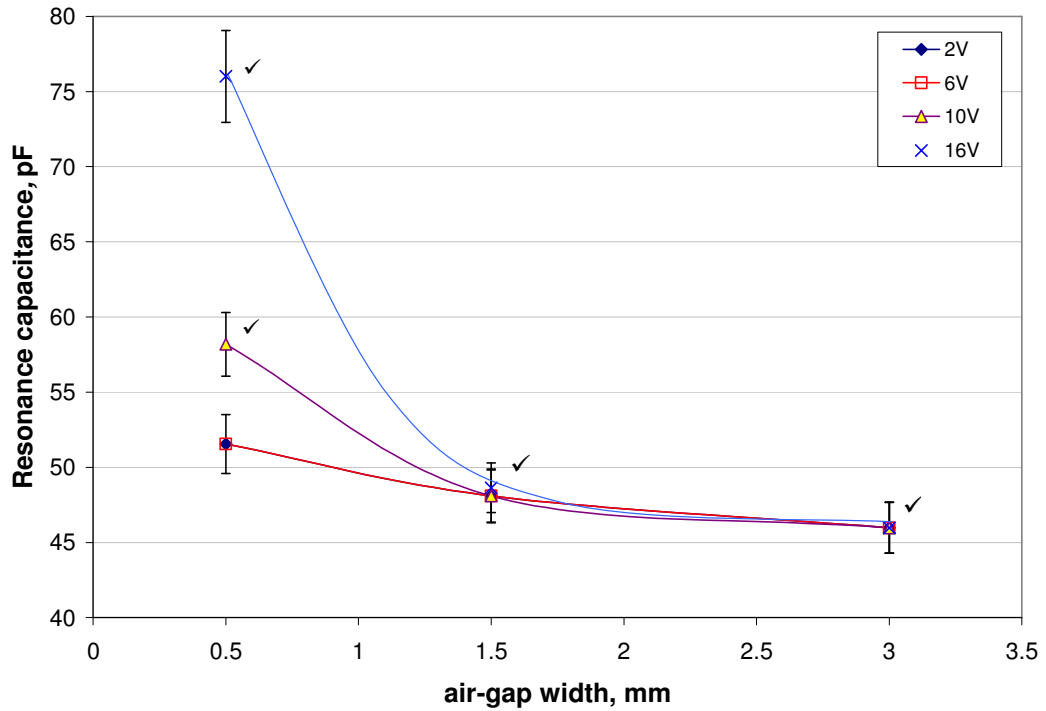


**Figure 4.9:** Capacitance of DBD at resonance deduced for different air-gap size (Alumina dielectric) at  $V_{DD} = 2V, 6V, 10V$  and  $16V$ . The ‘tick’ indicates breakdown of gap has occurred.

#### 4.1.1.4 Discharge voltage measured for various air-gap sizes with alumina dielectric barrier

The study is carried out for discharge frequency ranging from 100s Hz to 10kHz for DBD with alumina dielectric. The results are similar to those with glass dielectric.

##### **0.5mm air-gap**

Figure 4.10 shows the discharge voltage characteristics for air-gap 0.5mm at MOSFET driving voltage of  $V_{DD} = 16V$ . At  $f \leq 2.5kHz$ , ‘unipolar’ pulses are obtained while sine wave voltages at  $f \geq 6kHz$ , and resonance frequency is at 7kHz. The gap breaks down at discharge voltages  $\geq 6.2kV$ . The profiles of the discharge voltage at  $V_{DD} = 2V, 8V$ , and  $14V$  are compared in Figure 4.13. The magnitude of the ‘unipolar’

pulses increases when frequency is reducing towards  $10^2$ Hz, while the sinusoidal waveform amplitude peaks at resonant frequency of (7.0-8.5)kHz. Resonant frequency is higher for lower  $V_{DD}$  (when there is no visible microdischarge and gap capacitance is lower).

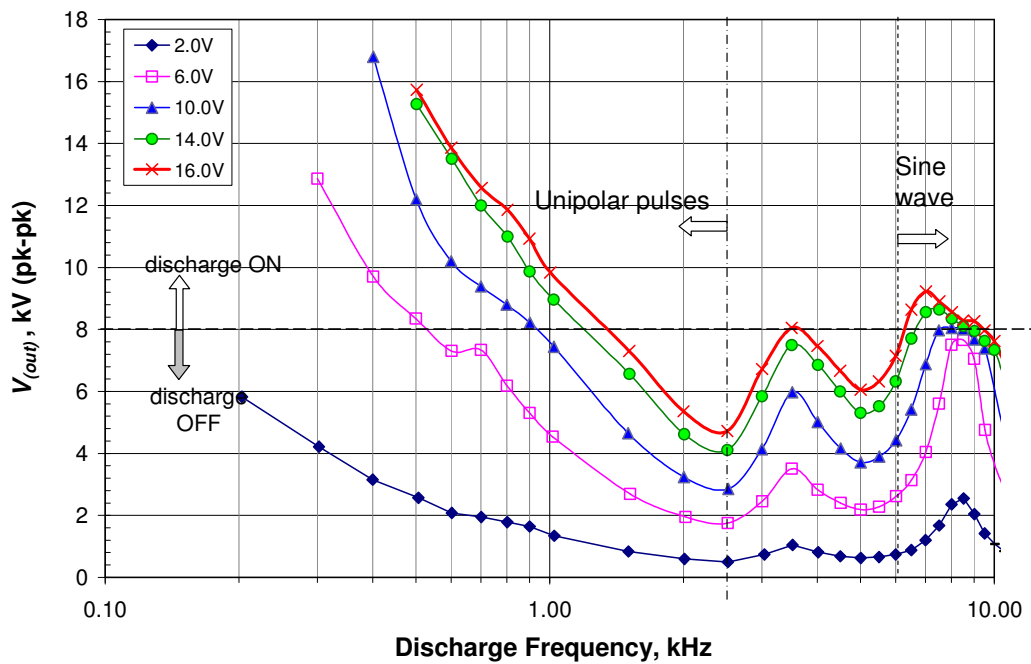


**Figure 4.10:** Discharge voltage (peak to peak) versus frequency for 0.5mm air-gap with alumina dielectric (at  $V_{DD} = 2.0\text{V}$ ,  $6.0\text{V}$ ,  $10.0\text{V}$ ,  $14.0\text{V}$ , and  $16.0\text{V}$ ).

### 1.5mm air-gap

Similar trends are observed for the 1.5mm air-gap as shown in Figure 4.11. “Unipolar” pulses are still obtained at  $f \leq 2.5\text{kHz}$  whilst sinusoidal voltages at  $f \geq 6.5\text{kHz}$ , and the resonance frequency is at slightly higher value of (8.5-9)kHz. The gap breaks down at higher discharge voltage (pk-pk)  $\sim 12\text{kV}$ .

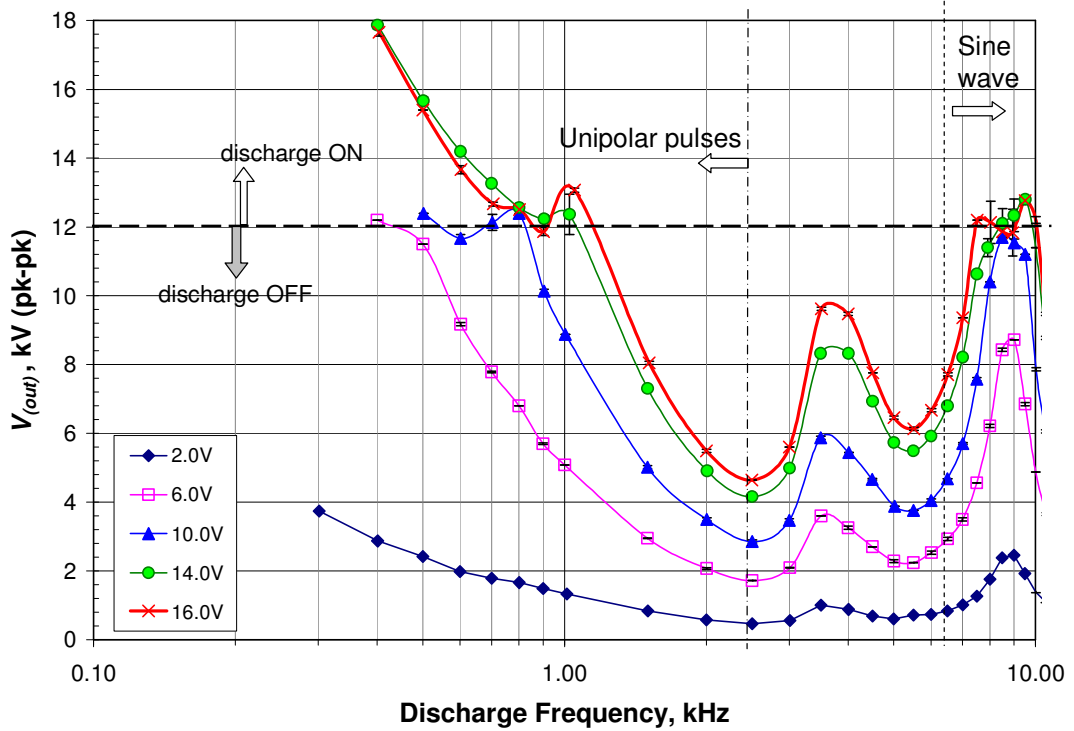


**Figure 4.11:** Discharge voltage (peak to peak) versus frequency for 1.5mm air-gap with alumina dielectric (at  $V_{DD} = 2.0\text{V}$ ,  $6.0\text{V}$ ,  $10.0\text{V}$ ,  $14.0\text{V}$ , and  $16.0\text{V}$ ).

### 3.0mm air-gap

Likewise in the case of 3.0mm air-gap with alumina dielectric (Figure 4.12), “unipolar” pulses and sinusoidal voltages are still obtained at same frequency ranges, and the resonance frequency is at 9kHz. No total breakdown in the gap occurs, just a few filamentary lines are observed at discharge voltage of ~21kV.

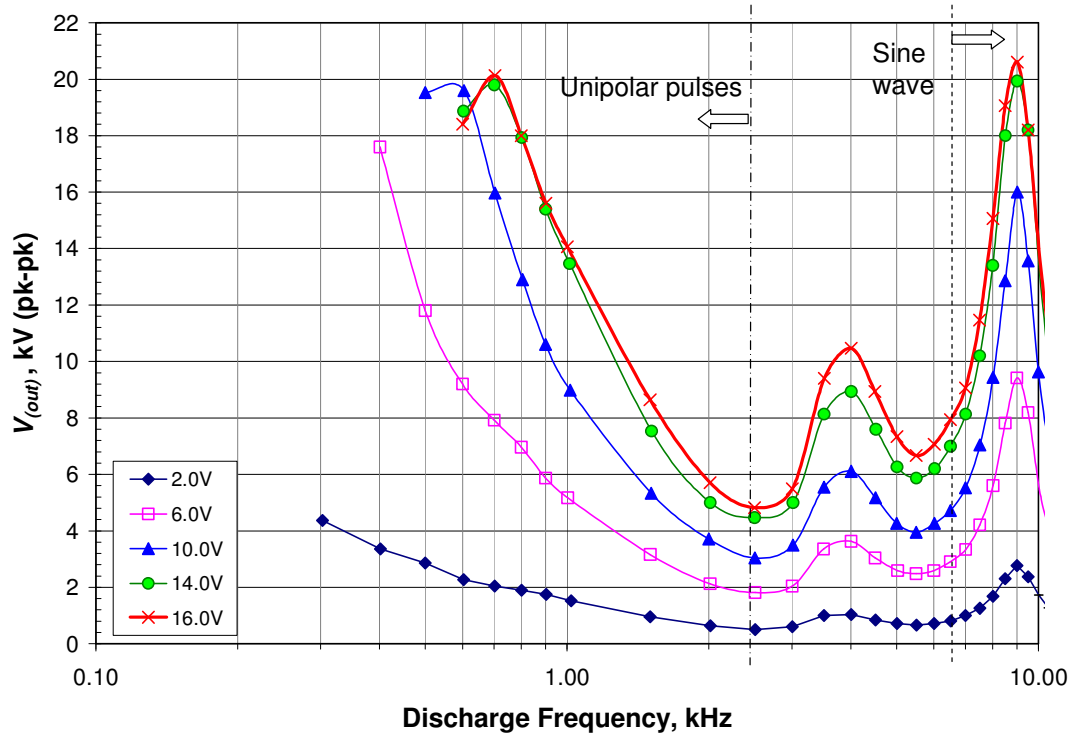


**Figure 4.12:** Discharge voltage (peak to peak) versus frequency for 3.0mm air-gap with alumina dielectric (at  $V_{DD} = 2.0V, 6.0V, 10.0V, 14.0V,$  and  $16.0V$ ).

#### 4.1.1.5 Comparison between Glass and Alumina Sheet as Dielectric Layer

To compare the discharge characteristic for glass and alumina dielectric, Figure 4.13 shows the overlay of voltage profiles for all three different air-gap sizes 0.5mm, 1.5mm, and 3.0mm for both materials. The solid line shows the results for glass sheet while the dashed lines are for alumina sheet. At frequency below 6kHz, the curves for glass and alumina dielectrics overlap each other for all the three air-gaps. The discharge profiles are relatively stable up to 6 kHz.

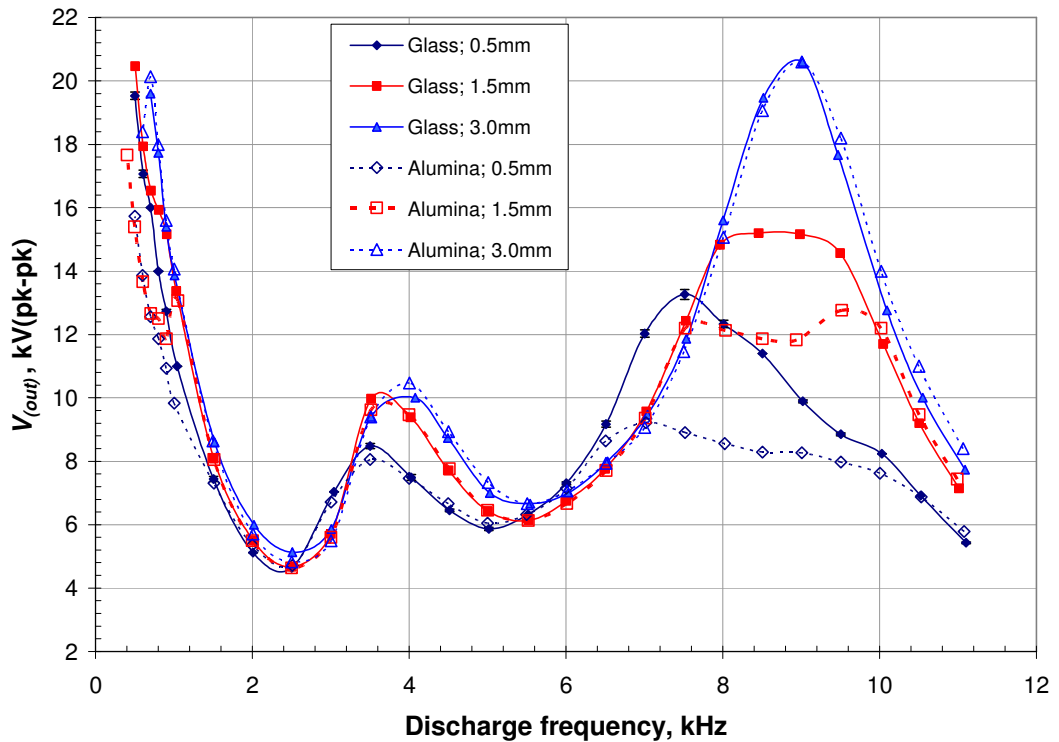


**Figure 4.13:** Comparison of peak to peak discharge voltage versus discharge frequency for all three 0.5, 1.5, 3.0mm air-gaps. (Glass and alumina dielectric;  $V_{DD} = 16.0V$ )

Glass DBD exhibited higher resonance frequency at 7.5kHz compared to alumina DBD (7.0kHz) for the 0.5mm air-gap. Discharge voltage at resonance is lower for the alumina DBD at both 0.5mm and 1.5mm air-gap. In the case of 3.0mm air-gap, both the alumina and glass resonance peaks are identical, occurring at 9kHz with peak-to-peak voltage of 21kV. Since their series capacitance deduced from resonance condition is almost the same (glass - 46pF, alumina - 47pF), the resonance frequency and peak voltage at resonance are expected to be the same for both alumina and glass DBDs (from Figures 4.3 and 4.9).

#### 4.1.2 Voltage and Current Signals for “Unipolar” Pulsed DBD

Typical discharge voltage and current waveforms obtained for “unipolar” pulsed DBD with 0.5mm air-gap and alumina dielectric is shown in Figure 4.14. Similar shapes are also obtained in DBD with glass dielectric and are not shown. The current waveform exhibits two regions of spurious spikes for every cycle. Dominantly positive current spikes occur at the first quadrant (rising positive voltage) of the voltage signal when the voltage level is sufficient to initiate breakdown. Dominantly negative current spikes, however, appear immediately after the steepest voltage fall region. The multi-spiked current signal is a signature of the filamentary nature of the DBD as reported by other investigators (Fang *et al.*, 2007, Kogelschatz, 2003). Averaging the current signal over 64 scans almost eliminates the current spikes (which appears randomly) allowing the capacitive current to be determined.

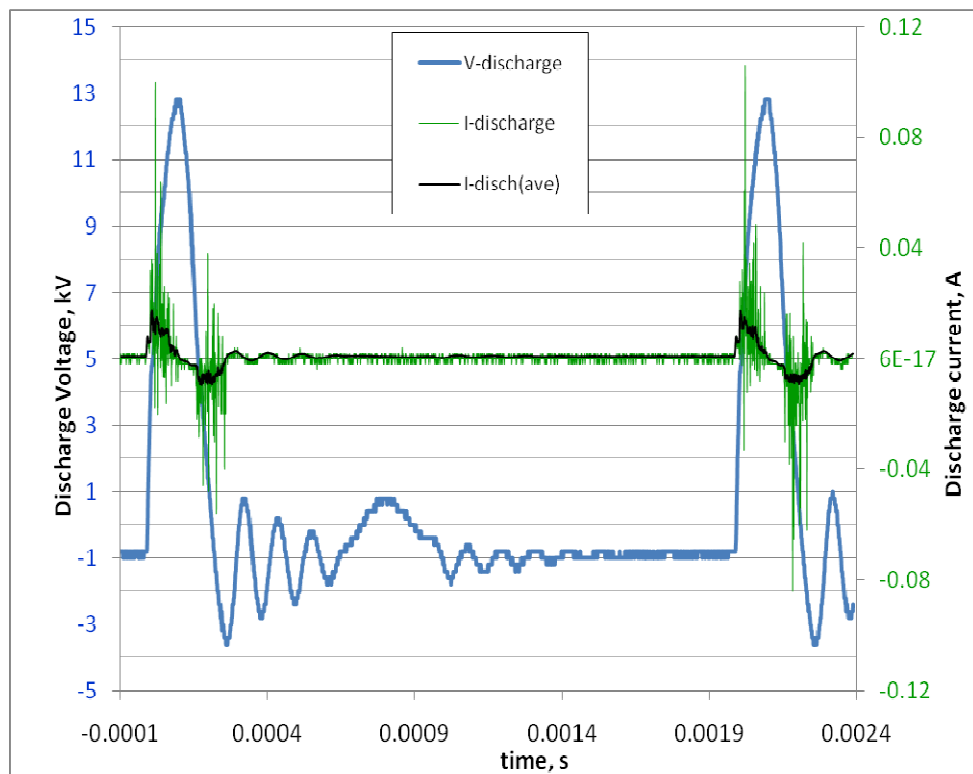


**Figure 4.14:** Typical voltage and current signals for 0.5mm air-gap in alumina DBD ( $V_{DD} = 16.0V$ ) at 500Hz (“unipolar” pulsed).



Figures 4.15(a)-(c) compare the voltage and current signals obtained for different air-gap widths in the “unipolar” pulsed DBD with alumina dielectric at 500Hz. The duration of the positive “unipolar” pulse is 250 $\mu$ s for the 0.5mm air-gap, narrows to 180 $\mu$ s as the air-gap increases to 3.0mm while the voltage peak gets higher. The time width of the negative overshoot of the pulse is (70-80) $\mu$ s with peak magnitude  $\leq 20\%$  of the positive peak. From these signals, various features are quantified and tabulated in Table 4.3.

The features tabulated in Table 4.3 are indicated in Figure 4.15(a). Initial (first) gradient of the rise in the positive “unipolar” pulse is the steepest and this portion corresponds to the charging of the DBD “capacitor” as evident in the transient current peak  $I_1^{(t)}$  followed by a flat displacement current of  $I_1$  (before breakdown). Capacitance  $C_1$  of this DBD “capacitor” (without conduction in the gap) is determined from the ratio of  $I_1$  to  $(dV/dt)_1$  and its value is larger but close to those estimated in Table 3.2, the difference ranging from 18% at the smallest gap to 50% at the largest gap.

The first gradient of the voltage rise above is the one that initiates the self-breakdown in the gap and it is steepest for the largest gap. The time from the start of the voltage pulse to the onset of breakdown  $\Delta t$  increases as the air-gap widens. Hence, the voltage build-up (or breakdown voltage) to first current spike,  $\Delta V_b$  increases correspondingly. The second gradient of the voltage rise  $(dV/dt)_2$  corresponds to the region where there are current filaments except at 3.0mm where only occasional current filaments are observed covering randomized small patches of the electrode surface (and at times the discharge is not ignited at all. The occasional current filament at the large gap is relatively larger in diameter tending to “arc” formation as evident from the very high initial current pulse accompanied by a large voltage dip as shown in Figure 4.15(c)

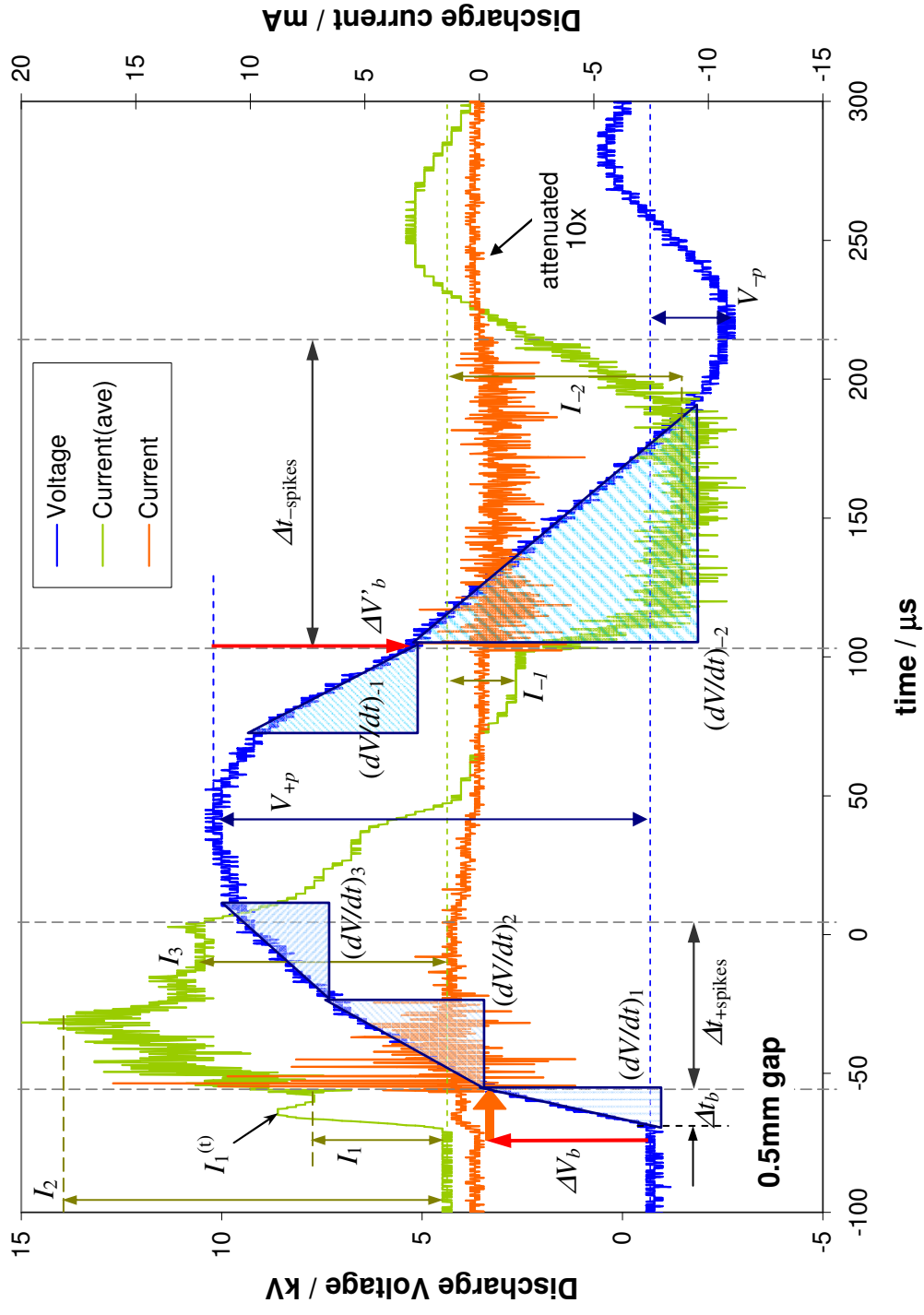


**Figure 4.15 (a):** Typical voltage and current signals in “unipolar” pulsed alumina DBD ( $V_{DD} = 16V$ ) at 500Hz for 0.5mm air-gap width.

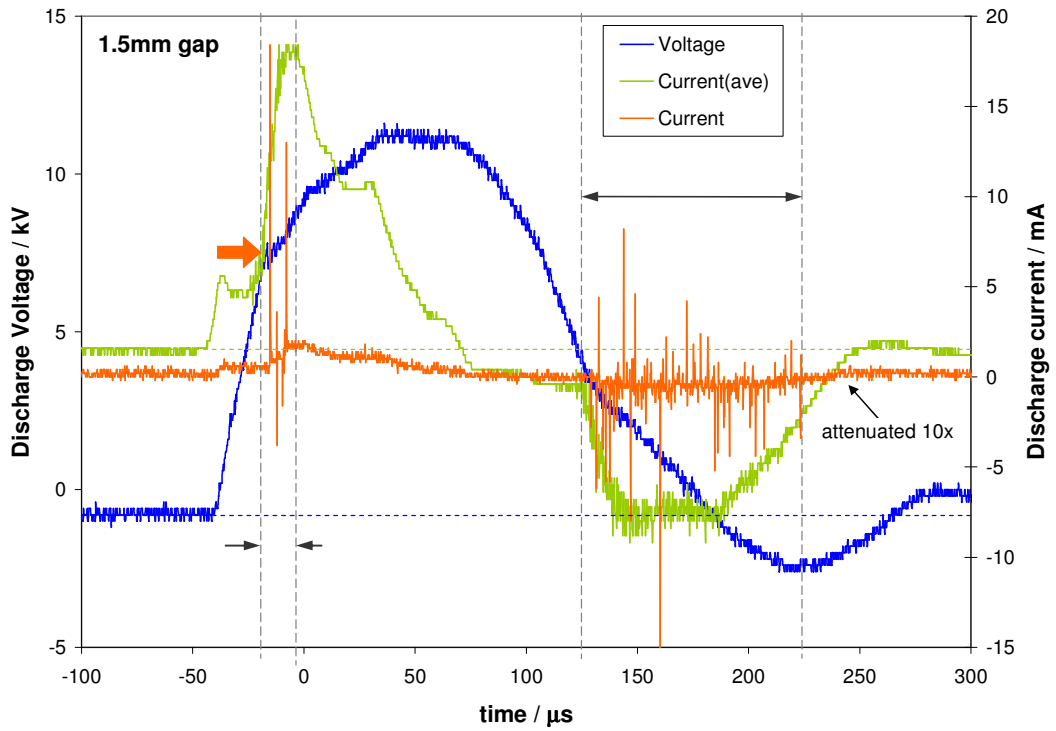


Figure 4.15 (b): Typical voltage and current signals in “unipolar” pulsed alumina DBD ( $V_{DD} = 16V$ ) at 500Hz for 1.5mm air-gap width.

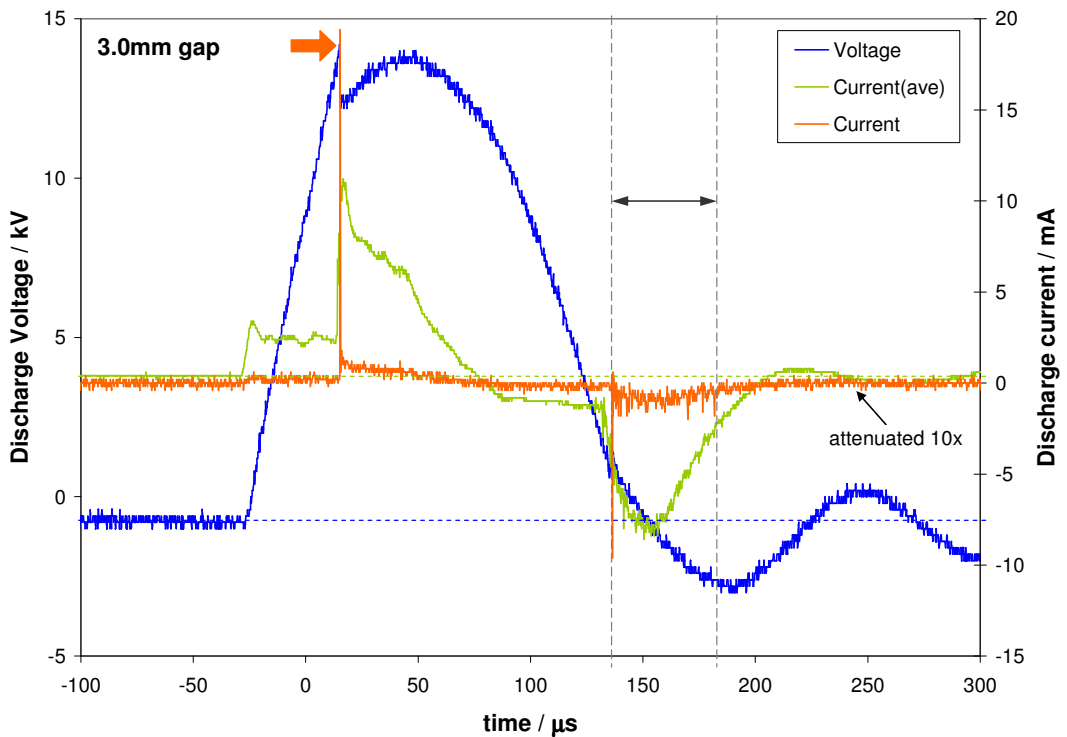
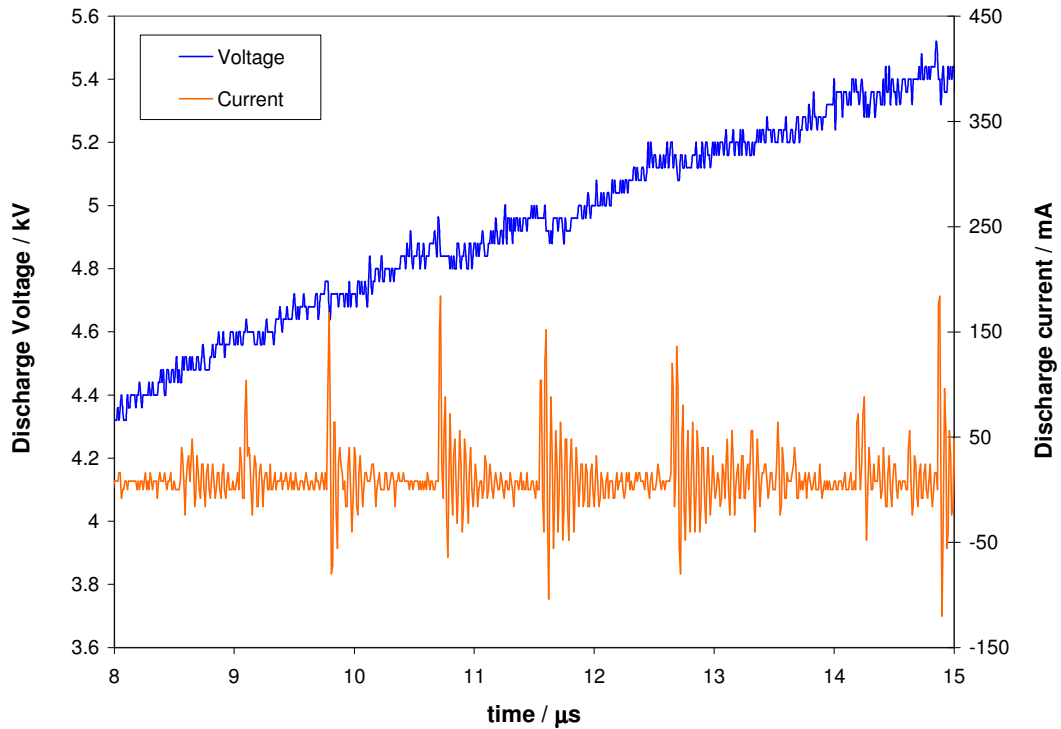


Figure 4.15 (c): Typical voltage and current signals in “unipolar” pulsed alumina DBD ( $V_{DD} = 16V$ ) at 500Hz for 3.0mm air-gap width.

**Table 4.3:** Various electrical features determined from the voltage and current signals of Figures 4.15(a)-(c).

No.	Properties of voltage and current signals	0.5mm; alumina	1.5mm; alumina	3.0mm; alumina
1	$(dV/dt)_1$ in kV/ $\mu$ s	0.299	0.373	0.437
2	$I_1^{(t)}$ in mA	7.4	4.1	2.9
3	$I_1$ in mA	5.8	3.1	2.1
4	Estimated $C_1 = I_1 / (dV/dt)_1$ in pF	19.4	8.3	4.8
5	$\Delta V_b$ in kV	+3.9	+7.7	+15
6	$\Delta t$ (0V to $V_b$ ) in $\mu$ s	13	24	43
7	$(dV/dt)_2$ in kV/ $\mu$ s	0.128	0.124	voltage dip by 1.6kV
8	$I_2$ in mA	15.8;	16.3;	10.8
9	$\Delta t_{+spikes}$ in $\mu$ s	64	10	single spike
10	$(dV/dt)_3$ in kV/ $\mu$ s	0.079	0.058	0.077
11	$I_3$ in mA	10.8	8.8	(7.5-5.8)
12	$V_{+p}$ in kV	10.9	11.9	14.6
13	Width of positive $V$ in $\mu$ s	247	224	178
<b>14</b>	<b>Peak power <math>P_{pk} = V_{+p}I_2</math> in W</b>	<b>172</b>	<b>194</b>	<b>158</b>
15	$(dV/dt)_{-1}$ in kV/ $\mu$ s	-0.137	-0.186	-0.240
16	$I_{-1}$ in mA	-2.9	-1.8	-1.5
17	Estimated $C_{-1} = I_{-1} / (dV/dt)_{-1}$ in pF	21.2	9.7	6.3
18	$\Delta V'_b$ in kV	-4.9	-7.8	-13
19	$(dV/dt)_{-2}$ in kV/ $\mu$ s	-0.083	-0.076	-0.108
20	$I_{-2}$ in mA	-9.4	-8.9	-8.1
21	$\Delta t_{-spikes}$ in $\mu$ s	113	98	47
22	$V_{-p}$ in kV	-1.9	-1.9	-2.1
23	Width of negative $V$ overshoot in $\mu$ s	83	83	70

The accompaniment of voltage dip to current spike is also evident at low current spike level as shown in Figure 4.16 for 0.5mm air-gap with alumina dielectric. Here, multiple current filaments are seen appearing at approximate rate of one per  $\mu\text{s}$ . Successive current spikes are possibly formed at locations other than site of previous current filament where field remains above breakdown.



**Figure 4.16:** Small current spikes accompanied by mild voltage dip in “unipolar” pulsed alumina DBD ( $V_{DD} = 16\text{V}$ ) at 500Hz with 0.5mm air-gap width.

The third gradient of voltage rise  $(dV/dt)_3$  occurring closer to the peak is the least steep. No current spikes are observed in this region for 1.5mm and 3.0mm air-gap. Though the voltage level is higher than the breakdown voltage, charge accumulation on the dielectric surface may have created a localized field that stops the growing current streamers from bridging the entire air-gap. Multiplying the peak voltage with the peak ‘capacitive’ current, the peak power  $P_{pk}$  in the DBD is found to be highest for the 1.5mm gap.

At the falling edge of the positive “unipolar” pulse, numerous negative current spikes could be observed when the voltage falls by  $\Delta V'_b$  from the peak value. The magnitude of  $\Delta V'_b$  approximates the breakdown voltage  $\Delta V_b$  at the rising edge. As the applied voltage decreases, the accumulated negative charges on the dielectric surface start to dissipate into the gap due to Coulomb force (repulsion among themselves and attraction to the positive ions which lagged behind near the grounded electrode), and move towards the grounded bare electrode. When the voltage falls sufficiently, these negatively-directed electrons can form filament that bridges the gap, giving rise to the negative current spikes. The capacitive current is also negative ( $i_C = C dV/dt$ ) due to the voltage fall. The delay from zero current to the onset of (negative) breakdown is rather constant at (55-60) $\mu$ s for all three air-gaps. This “second breakdown” of the air-gap due to the voltage induced by the accumulated charges on the surface of the dielectric during previous discharge (at the rising edge of the voltage) is similar to that described by Laroussi *et al* (2004).

Two regions of distinct gradient of voltage fall is identified, the first  $(dV/dt)_{-1}$  being steeper than the second  $(dV/dt)_{-2}$ . Capacitive current  $I_{-1}$  is determined at the steeper voltage fall region, and the capacitance  $C_{-1}$  is estimated.  $C_{-1}$  is higher than  $C_1$  (estimated from the rising edge) due to the accumulated charge on the dielectric surface which enhances its capacity. It is observed that the negative spikes generally have lower amplitude than the positive ones. The averaged negative current is also lower than the positive current and it falls with increased air-gap width. Though the duration of occurrence of negative spikes falls with increasing air-gap, it lasts longer than that for positive spikes.

Current and voltage signals for the ‘unipolar’ pulsed DBD with glass dielectric are also analyzed and tabulated in Table 4.4. The waveforms are not shown as they are similar to those of Figures 4.15. Similar features to those in alumina DBD are observed.

**Table 4.4:** Various electrical features determined from the ‘unipolar’ voltage and current signals of the DBD with glass dielectric. Grey highlight denotes no distinction in slope.

No.	Properties of voltage and current signals	0.5mm; glass	1.5mm; glass	3.0mm; glass
1	$(dV/dt)_1$ in kV/ $\mu$ s	0.345	0.337	0.276
2	$I_1^{(t)}$ in mA	6.8	4.1	2.9
3	$I_1$ in mA	4.6	2.9	2.0
4	Estimated $C_1 = I_1 / (dV/dt)_1$ in pF	13.3	8.6	7.2
5	$\Delta V_b$ in kV	+3.9	+8.7	+15.8
6	$\Delta t$ (0V to $V_b$ ) in $\mu$ s	11	26	45
7	$(dV/dt)_2$ in kV/ $\mu$ s	0.213	0.201	0.054
8	$I_2$ in mA	5.0-5.7	5.1	3.2
9	$\Delta t_{+spikes}$ in $\mu$ s	80	55	30
10	$(dV/dt)_3$ in kV/ $\mu$ s	0.136	0.098	0.054
11	$I_3$ in mA	3.1-3.8	1.8-2.6	1.9
12	$V_{+p}$ in kV	14.2	15.3	17.2
13	Width of positive $V$ in $\mu$ s	193	182	163
14	<b>Peak power <math>P_{pk} = V_{+p}I_2</math></b>	<b>71-81</b>	<b>78</b>	<b>55</b>
15	$(dV/dt)_{-1}$ in kV/ $\mu$ s	-0.177	-0.224	-0.225
16	$I_{-1}$ in mA	-3.1	-2.1	-(1.6-1.9)
17	Estimated $C_{-1} = I_{-1} / (dV/dt)_{-1}$ in pF	17.5	9.4	7.1-8.4
18	$\Delta V'_b$ in kV	-5.5	-9.7	-17.2
19	$(dV/dt)_{-2}$ in kV/ $\mu$ s	-0.177	-0.161	-0.134
20	$I_{-2}$ in mA	-(4.0-4.5)	-3.4	-2.5
21	$\Delta t_{-spikes}$ in $\mu$ s	85	68	36
22	$V_{-p}$ in kV	-3.6	-3.5	-3.9
23	Width of negative $V$ overshoot in $\mu$ s	68	63	64

### 4.1.3 Voltage and Current Signals for Sinusoidal Voltage Powered DBD

The discharge voltage and current waveforms for sinusoidal voltage powered DBD with 0.5mm air-gap and alumina dielectric is shown in Figures 4.17. Waveforms for DBD with glass dielectric are similar (not shown). Again, the current waveform exhibits two regions of spurious spikes for every cycle, the positive current spikes at the first quadrant while the negative current spikes at the third quadrant (negative) of the voltage signal. The multi-spiked current signal again signifies filamentary nature of the discharge.

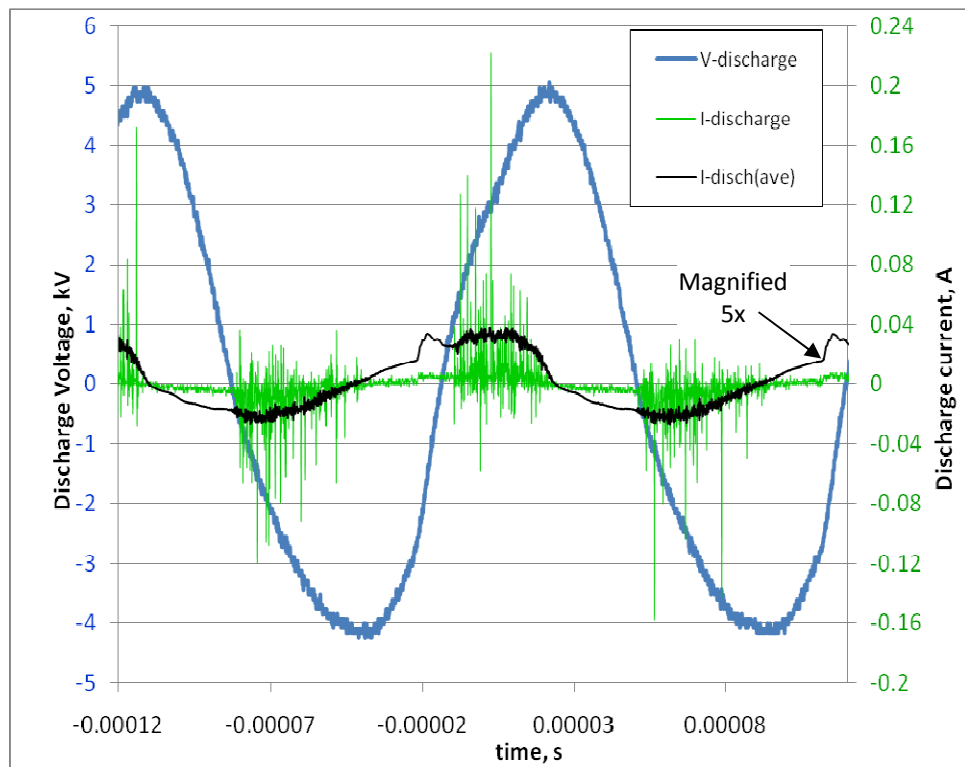


**Figure 4.17:** Typical voltage and current signals for 0.5mm air-gap in alumina DBD ( $V_{DD} = 16.0V$ ) at 7.5kHz (sinusoidal voltage).

These waveforms for different air-gap widths in alumina DBD are shown in Figures 4.18(a)-(c), from which various features are also quantified and tabulated in Table 4.5.



**Table 4.5:** Various electrical features determined from the sinusoidal voltage and current signals of Figures 4.18(a)-(c). Grey highlight denotes the same slope.

No.	Properties of voltage and current signals	0.5mm; alumina	1.5mm; alumina	3.0mm; alumina
1	$(dV/dt)_1$ in kV/ $\mu$ s	0.319	0.281	0.334
2	$I_1^{(t)}$ in mA	8.4	3.9	3.0
3	$\Delta V_b$ in kV	+4.3	+6.6	+8.4
4	$\Delta t$ (Vmin to $V_b$ ) in $\mu$ s	23	35	33
5	$(dV/dt)_2$ in kV/ $\mu$ s	0.139	0.231	0.334
6	$I_2$ in mA	8.0	3.6; 7.5 (strong spike)	3.0
7	$\Delta t_{+spikes}$ in $\mu$ s	34	29	20; sparsely
8	$V_{+p}$ in kV	4.5	5.6	8.8
9	Width of positive $V$ in $\mu$ s	67	60	59
10	Peak power $P_{pk} = V_{+p}I_2$	36	20; 42	26
11	$(dV/dt)_{-1}$ in kV/ $\mu$ s	-0.201	-0.326	-0.463
12	$\Delta V'_b$ in kV	-3.7	-5.5	-7.6
13	$(dV/dt)_{-2}$ in kV/ $\mu$ s	-0.128	-0.220	-0.257
14	$I_{-2}$ in mA	-8.8	-2.4	-2.6
15	$\Delta t_{-spikes}$ in $\mu$ s	48	35	26, sparsely
16	$V_{-p}$ in kV	-4.0	-5.5	-8.0
17	Width of negative $V$ in $\mu$ s	67	63	60
18	Frequency $f_{sine}$ in kHz	7.5	8.1	8.4

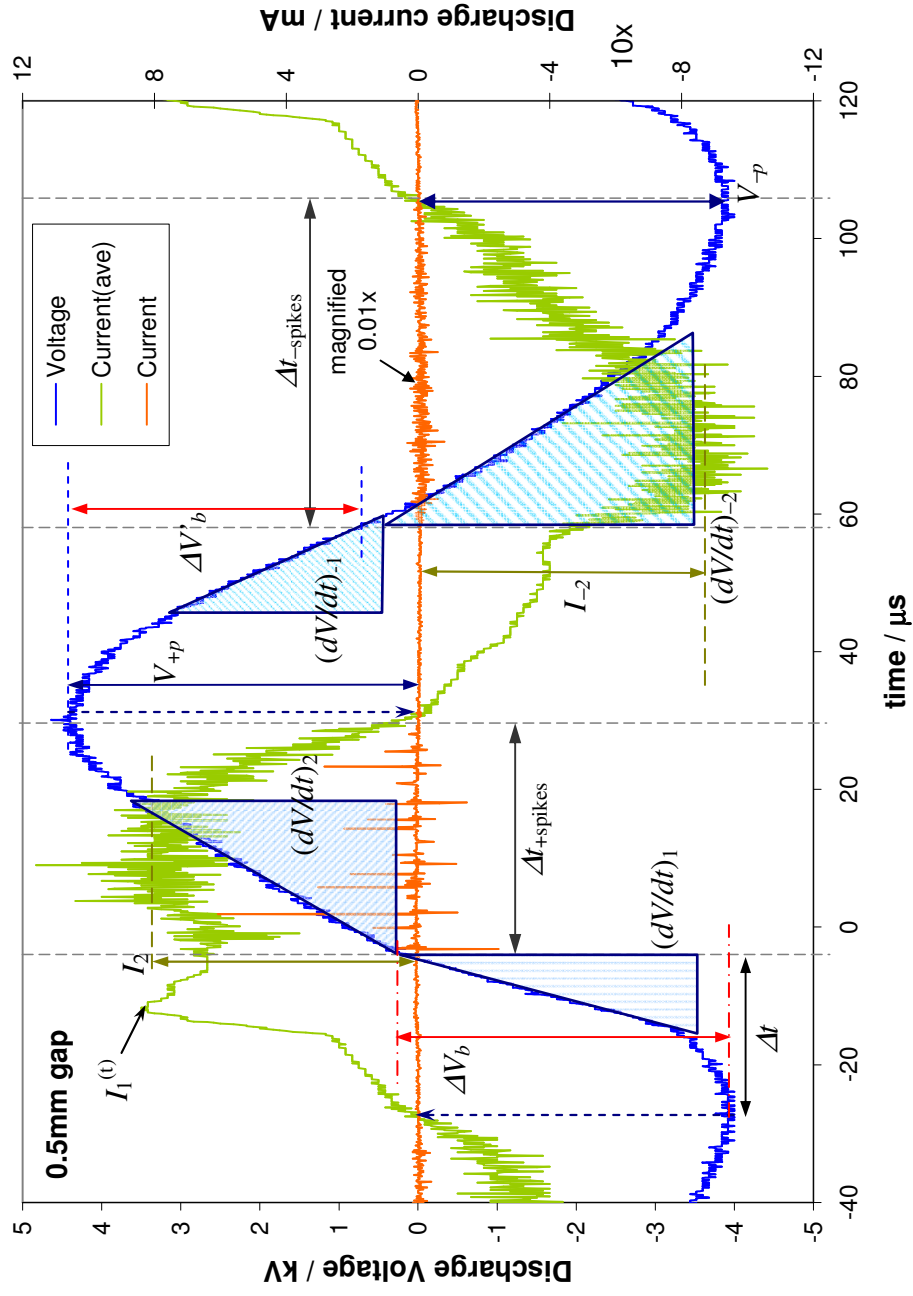


**Figure 4.18(a):** Typical voltage and current signals in sinusoidal voltage powered alumina DBD ( $V_{DD} = 16V$ ) at resonance for 0.5mm air-gap width.

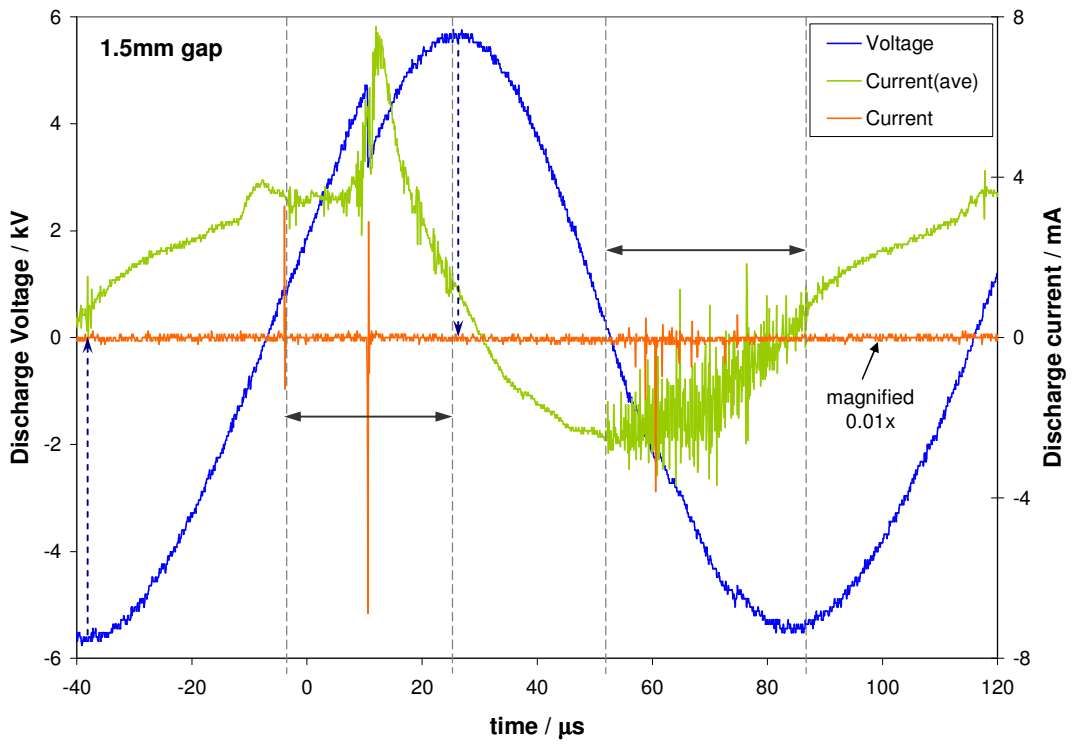


**Figure 4.18(b):** Typical voltage and current signals in sinusoidal voltage powered alumina DBD ( $V_{DD} = 16V$ ) at resonance for 1.5mm air-gap width.

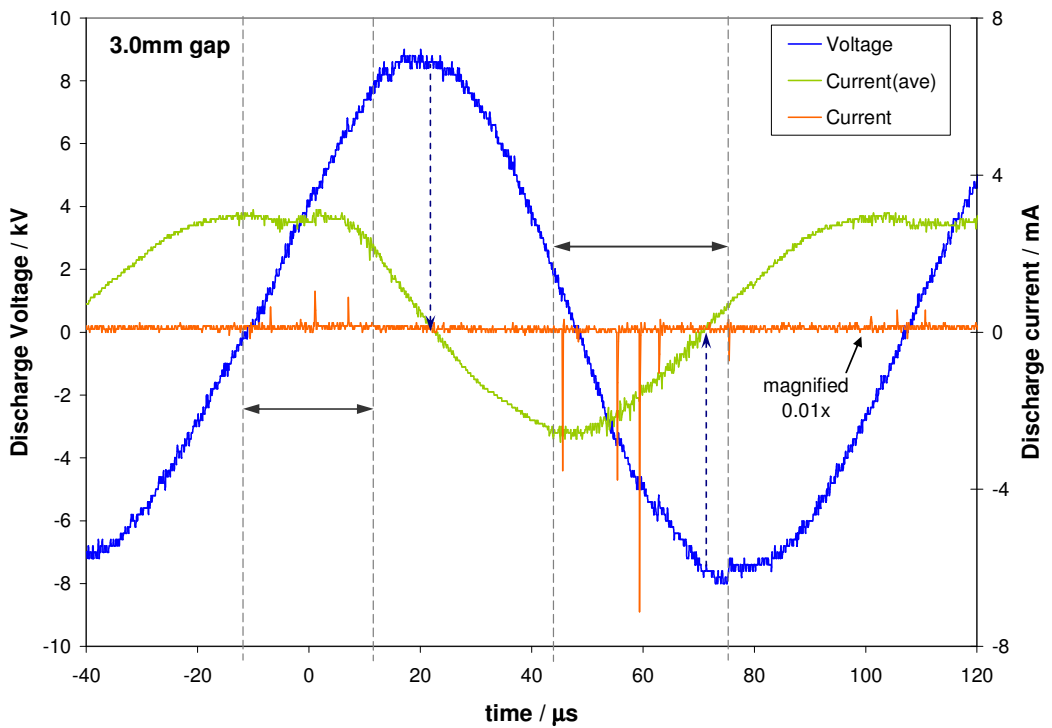


**Figure 4.18(c):** Typical voltage and current signals in sinusoidal voltage powered alumina DBD ( $V_{DD} = 16V$ ) at resonance for 3.0mm air-gap widths.

In the case of sinusoidal voltage, only two gradients in the voltage rise are identified, the steeper one  $(dV/dt)_1$  corresponding to pre-formation of current filaments. It is followed by a smaller gradient  $(dV/dt)_2$  where numerous microdischarges (or current filaments) are present (Figure 4.18(a)). The rise in voltage required to reach breakdown of the gap  $\Delta V_b$  is comparable to those registered for “unipolar” pulsed DBD for the smaller air-gaps but is appreciably lower in the 3.0mm air-gap. Similar trend is also observed for the drop in voltage on the falling edge of the voltage signal. Strong current spike is observed in the 1.5mm air-gap which is accompanied by a large dip in the voltage signal. This contributes to the highest peak power registered though the peak (positive and negative) voltage increases with air-gap width. However, the magnitude of the peak power is 5-10 times lower than those in the “unipolar” pulsed DBD with alumina dielectric as shown in Figure 4.19.

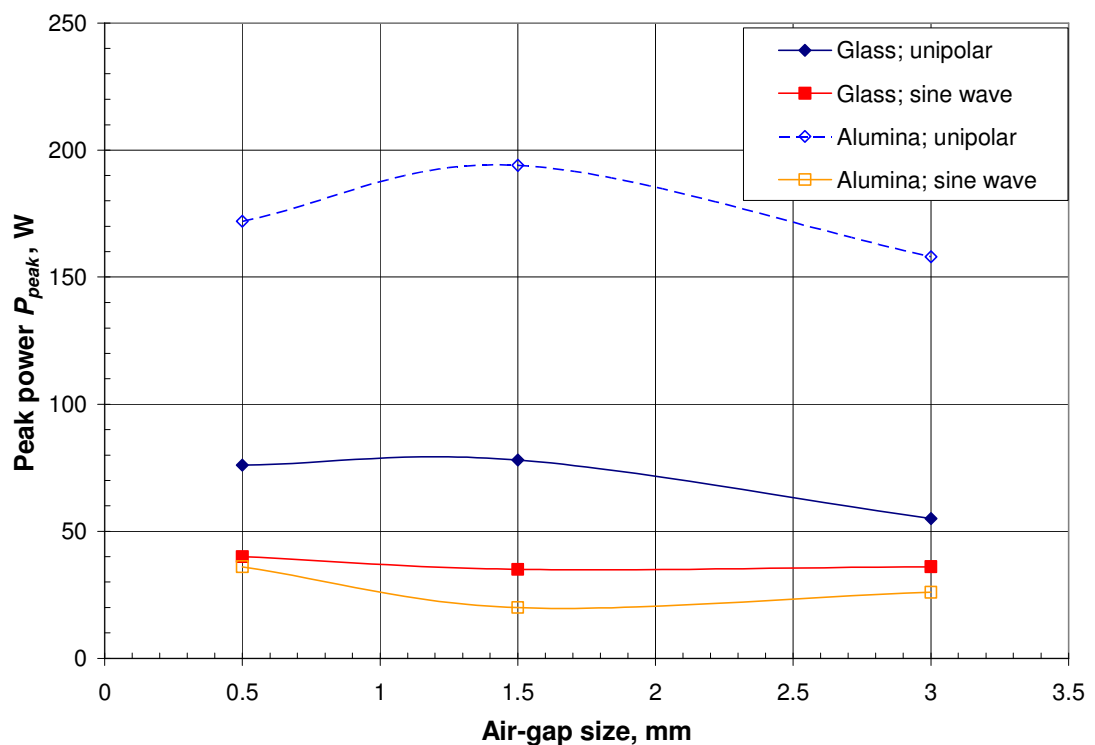


**Figure 4.19:** Variation of peak power in the DBD with air-gap size for glass and alumina dielectrics at “unipolar” pulsed and sine wave voltages.

In the case of DBD with glass dielectric powered by sinusoidal voltage, similar features to those with alumina dielectric are observed, and hence, are not shown. However, the results from the analysis of the current and voltage signals are tabulated in Table 4.6.

**Table 4.6:** Various electrical features determined from the sinusoidal voltage and current signals of the DBD with glass dielectric.

No.	Properties of voltage and current signals	0.5mm; glass	1.5mm; glass	3.0mm; glass
1	$(dV/dt)_1$ in kV/ $\mu$ s	0.409	0.452	0.677
2	$I_1^{(t)}$ in mA	7.7	4.1	3.9
3	$\Delta V_b$ in kV	+5.4	+9.0	+8.0
4	$\Delta t$ ( $V_{min}$ to $V_b$ ) in $\mu$ s	25	32	24
5	$(dV/dt)_2$ in kV/ $\mu$ s	0.273	0.296	0.479
6	$I_2$ in mA	5.4	4.8	3.9
7	$\Delta t_{+spikes}$ in $\mu$ s	38	25	21
8	$V_{+p}$ in kV	7.4	7.2	9.2
9	Width of positive $V$ in $\mu$ s	66	56	54
<b>10</b>	<b>Peak power <math>P_{pk} = V_{+p}I_2</math></b>	<b>40</b>	<b>35</b>	<b>36</b>
11	$(dV/dt)_{-1}$ in kV/ $\mu$ s	-0.369	-0.413	-0.499
12	$I_{-1}^{(t)}$ in mA	-6.1	-3.2	-2.9
13	$\Delta V'_b$ in kV	-6.3	-9.2	-11.2
14	$(dV/dt)_{-2}$ in kV/ $\mu$ s	-0.306	-0.255	-0.379
15	$I_{-2}$ in mA	-5.6	-2.9	-2.5
16	$\Delta t_{-spikes}$ in $\mu$ s	41	29	26
17	$V_{-p}$ in kV	-6.7	-6.4	-8.0
18	Width of negative $V$ in $\mu$ s	65	60	57
19	Frequency $f_{sine}$ in kHz	7.6	8.6	9.0

#### 4.1.4 Current spikes

On close scrutiny of a single current spike in Figure 4.20, the main peak usually has a width of  $\sim 20\text{ns}$  (FWHM) followed by a ringing tail (under-damped) in all DBD configuration studied presently. The  $20\text{ns}$  time duration of a microdischarge filament is typical of DBD in atmospheric air (Gibalov and Pietsch, 2000). As long as the rate of voltage rise is not above  $500\text{kV}/\mu\text{s}$ , the shape of the current spike of a single microdischarge is independent of the power supply or waveform of applied voltage. The quenching of a microdischarge channel is a self-arresting effect of the dielectric barrier due to charge accumulation at its surface. This causes a local collapse of the electric field in the area defined by the surface charge.

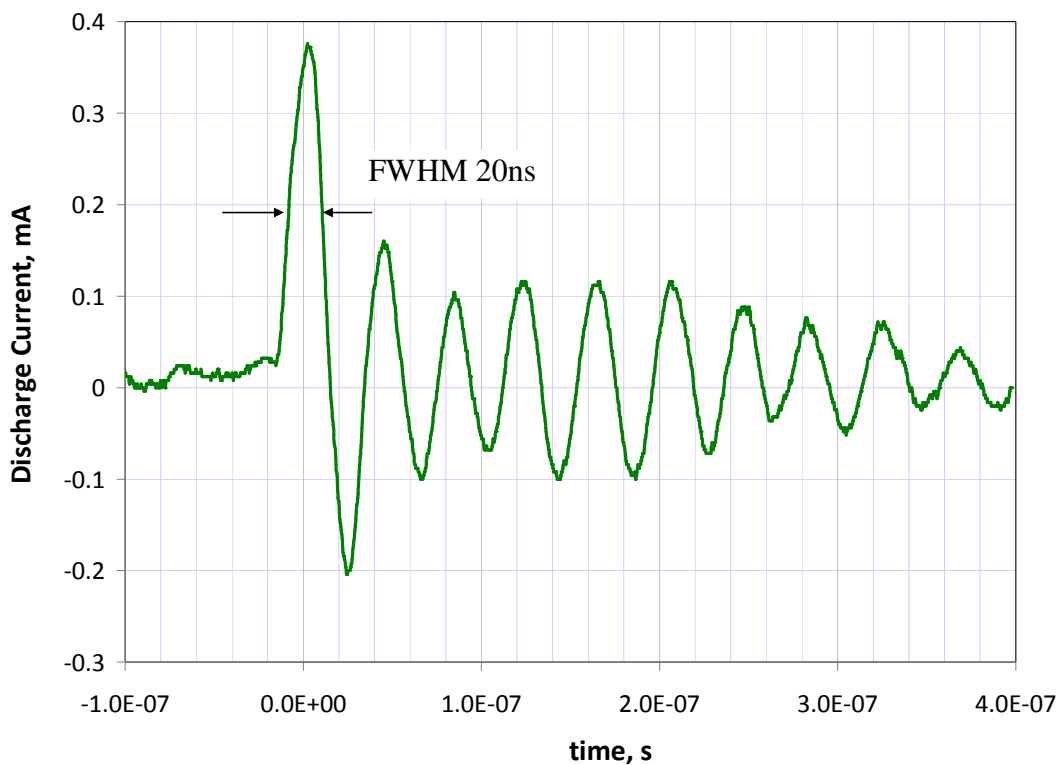


**Figure 4.20:** Current spike in alumina DBD with 0.5mm air-gap under “unipolar” pulsed excitation (500Hz).

It is observed that the smallest gap exhibits current spikes of lower amplitude but higher production rate of current spikes that occur for longer duration irrespective whether it is positive or negative spikes. These are shown in Figures 4.21 and 4.22 for positive and negative current spikes respectively under sinusoidal voltage excitation in DBD with alumina dielectric. All signals are obtained with applied voltage driven at  $V_{DD} = 16V$ . Hence, smaller gap supports more diffuse-like or homogeneous DBD which can also be physically observed in Figures 4.25 and 4.26. Comparison of number of spikes for different DBD and voltage excitation at fixed air-gap is shown in Figure 4.23. Alumina DBD exhibits higher production rate of current spikes. Both type of voltage excitation seems to give comparable production rate.

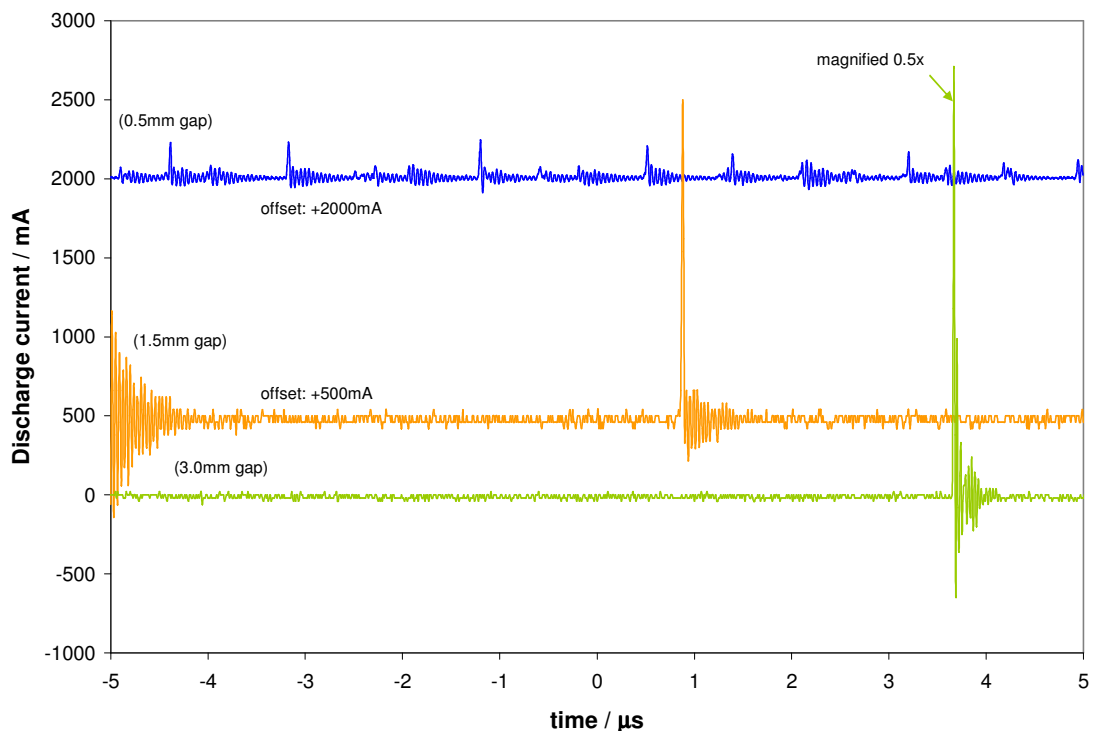


**Figure 4.21:** Typical signal of the current spikes at **positive** voltage excitation (sinusoidal voltage at resonance) for 0.5, 1.5, and 3.0mm air-gap widths in alumina DBD. The two upper signals are offset for clarity and the lowest signal is attenuated 2×.

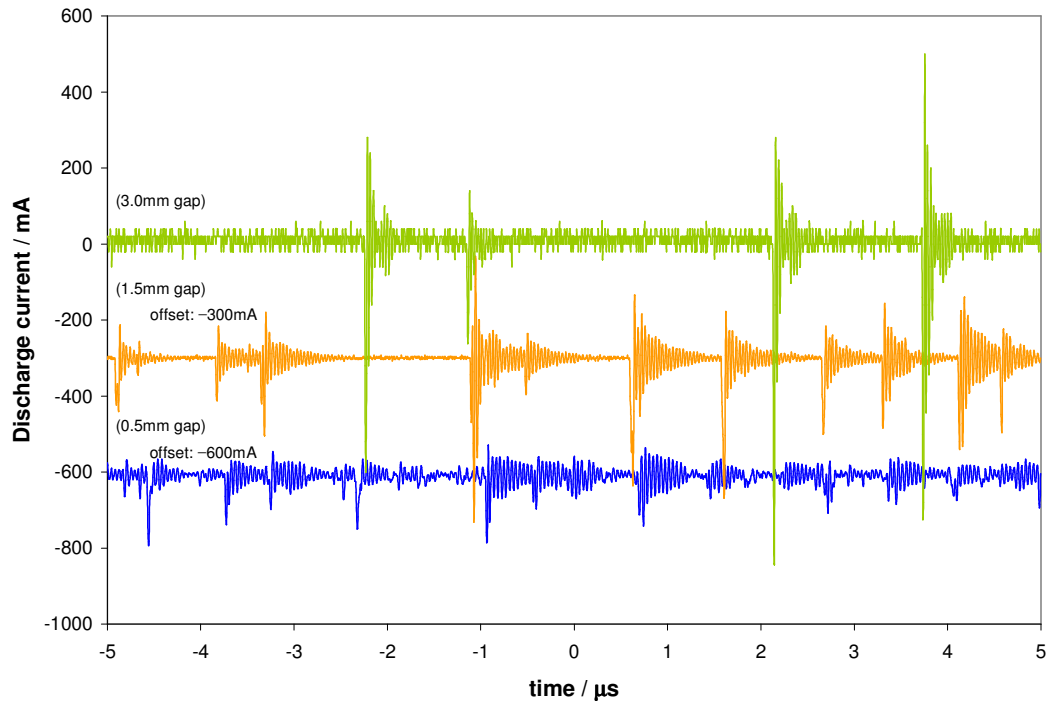


**Figure 4.22:** Typical signal of the current spikes at **negative** voltage excitation (sinusoidal voltage at resonance) for 0.5, 1.5, and 3.0mm air-gap widths in alumina DBD. The two lower signals are offset for clarity.

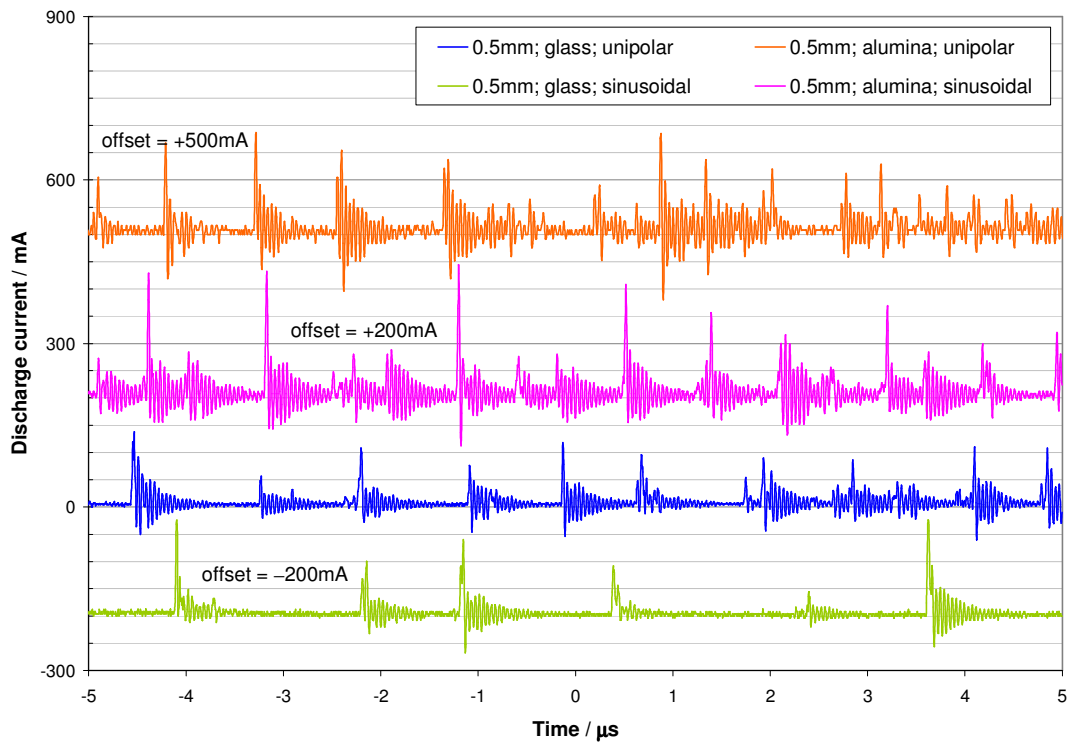


**Figure 4.23:** Comparing the positive current spikes for glass and alumina DBDs with 0.5mm air-gap width ( $V_{DD} = 16V$ ) powered by “unipolar” pulses at 500Hz and sinusoidal voltage at resonance frequency (7.5-8.5kHz).



To quantify the deduction above, the number of total positive ( $N_+$ ) and negative ( $N_-$ ) current spikes is counted for each cycle to estimate the microdischarge density and the result is shown in Figure 4.24. Hence, it can be concluded that the alumina DBD with 0.5mm air-gap powered by sinusoidal voltage produces a discharge that is most diffuse-like or homogeneous.

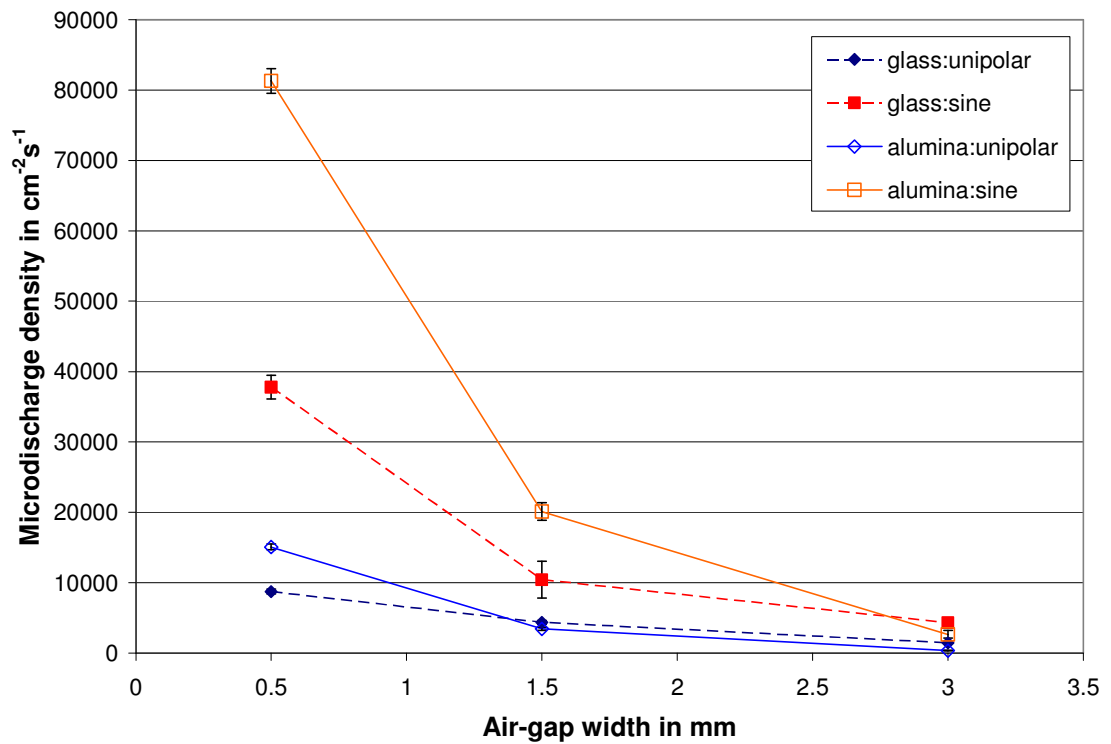


**Figure 4.24:** Dependence of microdischarge density with air-gap size for glass and alumina dielectrics at “unipolar” pulsed and sine wave voltages.

## 4.2 Physical Appearance of the Discharge

The discharge (filamentary or diffuse-like) produced in the air-gap is imaged via a Canon EOS 40D digital SLR camera. Images are captured for the glass and alumina DBD at three air-gap sizes of 0.5mm, 1.5mm, and 3.0mm powered by “unipolar” pulses and sinusoidal voltage. The images are shown in Figures 4.25 to 4.29. Frequency of operation for the “unipolar” pulsed DBD is 500Hz; while the sinusoidal voltage is at 8.5kHz. For better image quality, the aperture size, shutter speed and sensitivity of the camera are adjusted accordingly.

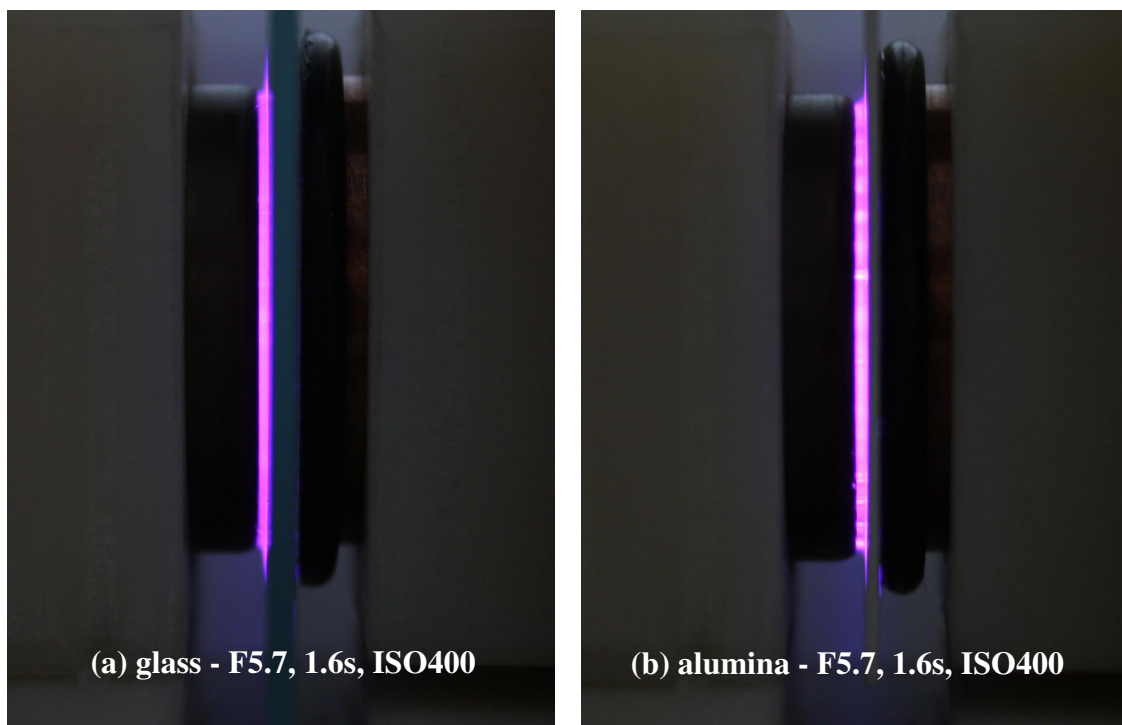


**Figure 4.25:** 0.5mm air-gap. Physical appearance of the discharge at 500Hz (“unipolar” pulses) with glass and alumina dielectric barriers.

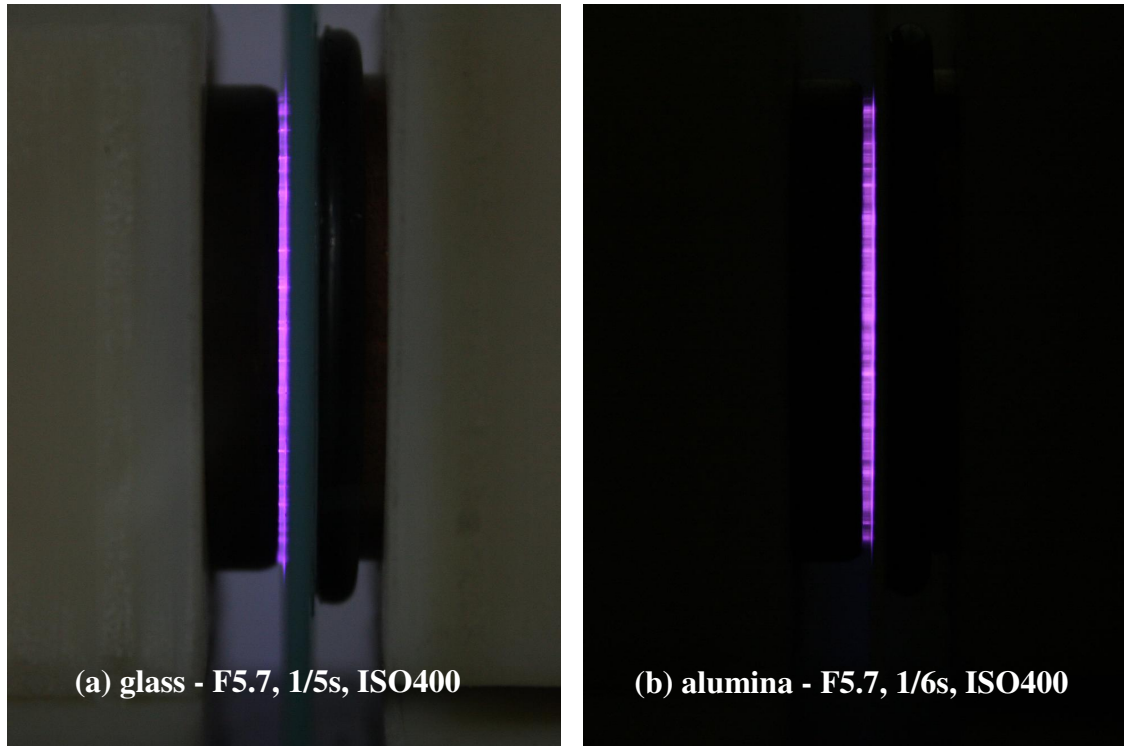


**Figure 4.26:** 0.5mm air-gap. Physical appearance of the discharge at 8.5kHz (sinusoidal voltage) with glass and alumina dielectric barriers.

For the 0.5mm air-gap at 500Hz (“unipolar” pulses), the discharge appears stable and diffuse-like (Figure 4.25) for both type of dielectric barriers though some stronger (brighter) filaments across the gap are evident in alumina for the indicated exposure time. At 8.5kHz sinusoidal voltage excitation (Figure 4.26), both discharges show some current filaments over a background of diffuse plasma though discharge in alumina dielectric appears more filamentary.

At larger air-gap of 1.5mm, the discharge is distinctly filamentary for all conditions (Figures 4.27 and 4.28) stated. The filaments seem to be more evenly distributed in the case of glass compared to alumina. For the widest air-gap of 3.0mm (Figure 4.29), only the image of filamentary discharge excited by “unipolar” pulse was captured. No breakdown was imaged for the sinusoidal voltage discharge though unstable current filaments are sometimes observed jumping over the surface in patches.

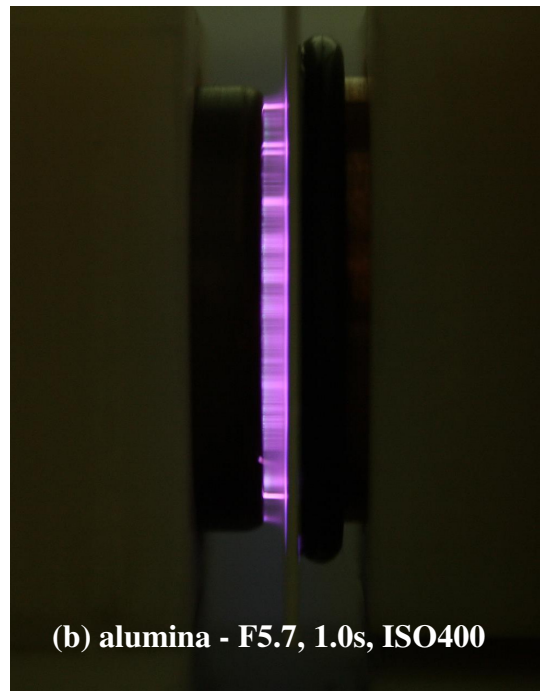
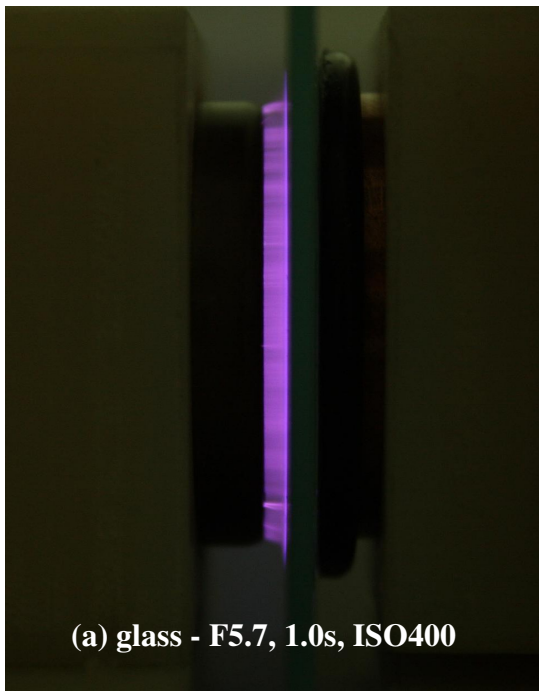


**Figure 4.27:** 1.5mm air-gap. Physical appearance of the discharge at 500Hz (“unipolar” pulses) with glass and alumina dielectric barriers.

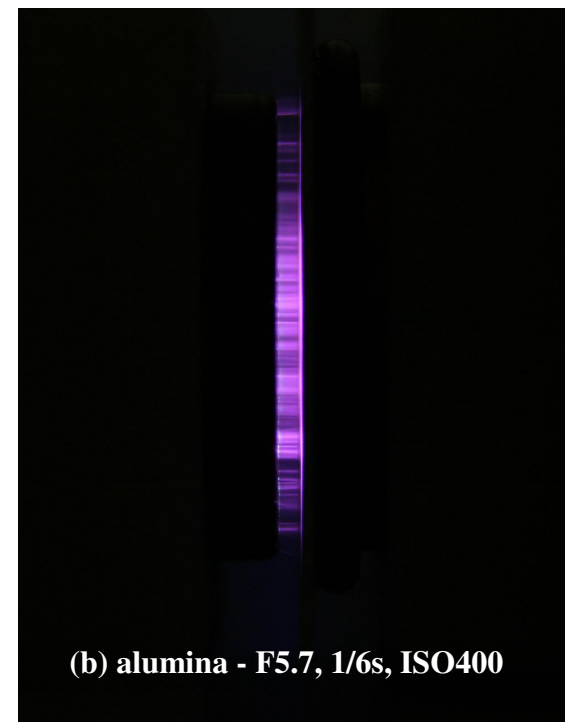
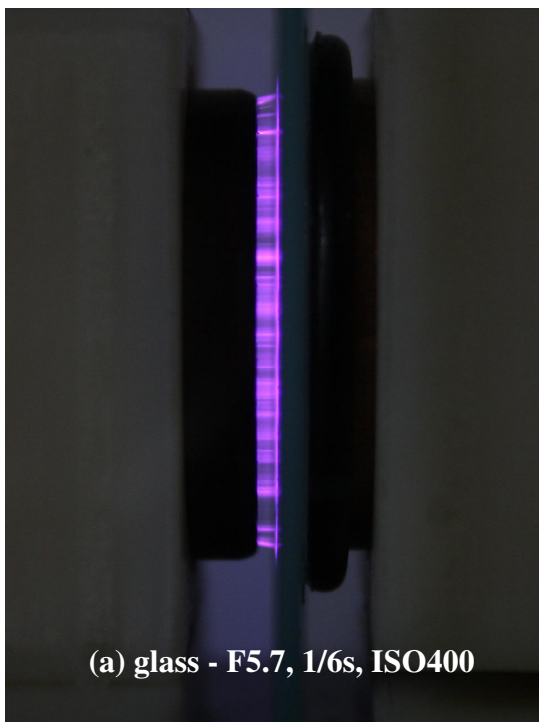


**Figure 4.28:** 1.5mm air-gap. Physical appearance of the discharge at 8.5kHz (sinusoidal voltage) with glass and alumina dielectric barriers.

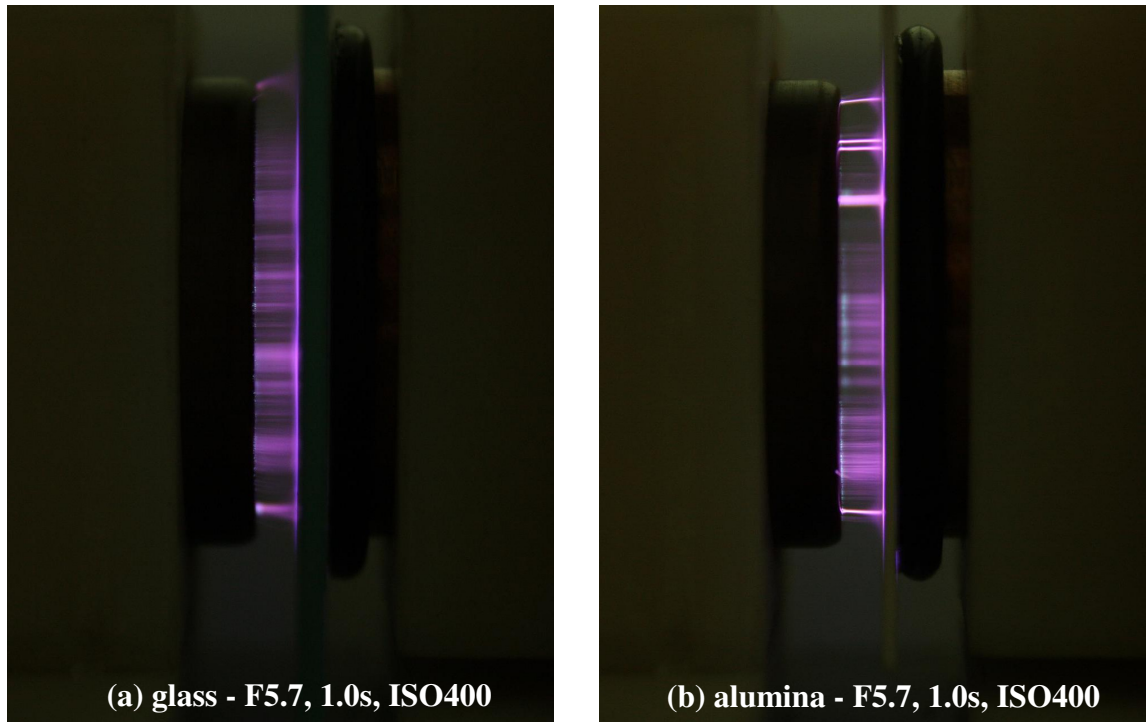


**Figure 4.29:** 3.0mm air-gap. Physical appearance of the discharge at 500Hz (“unipolar” pulses) with glass and alumina dielectric barriers.

It can be seen that discharge in smaller air-gap tends to distribute its microdischarges more evenly over the available surface, giving the appearance of a diffuse and uniform background glow with some “blurred” filaments spread evenly over the electrode surface. Glass dielectric appears to produce less intense filaments compared to alumina. This may be partly due to the larger amplitude current spikes in alumina dielectric as shown in Figure 4.23 which is supported by its larger capacitance.

On the dependence on voltage pulse shape, the 8.5kHz sinusoidal voltage DBD appears to produce more filamentary appearance than 500Hz “unipolar” pulsed DBD. The exposure time for the pictures taken was (1.0-1.6)s for the “unipolar” pulsed discharge and (167-200)ms for the sinusoidal voltage DBD. Life time of single microdischarge is 20ns (Figure 4.20), terminated due to charge accumulation on the dielectric surface. If these microdischarges are randomly distributed spatiotemporally,

captured image of the discharge over the timescale stated above would be blurred. However, if the microdischarges were to strike at the same spot over many cycles, then distinct filament could be captured. This is due to memory effect (Fridman, 2005a) of the dielectric due to the slow dissipation of positive ions in the volume (microdischarge remnant  $\sim 10\mu\text{s}$ ) that facilitates new microdischarges to reignite at the same spot as the polarity of the applied voltage changes. The “unipolar” pulse in this case is not truly uni-polarity. About  $130\mu\text{s}$  after the positive peak, the voltage pulse reverses in polarity due to a small negative over-shoot. In the case of sinusoidal voltage at  $8.5\text{kHz}$ , the voltage reverses in polarity approximately  $30\mu\text{s}$  after the positive peak. Hence, the “unipolar” pulse allows more time for the positive charges in the volume to dissipate during the “OFF” time. Hence, the formation of filaments due to memory effect is more prominent in the sinusoidal voltage DBD.

### 4.3 Spectral Emission from the DBD

The Ocean Optics HR4000 spectrometer is employed to measure the emission spectra from the DBD and the arrangement was shown in Figure 3.8. The air-gap is fixed at  $1.5\text{mm}$  while the discharge is operated with (i) “unipolar” pulsed DBD at  $500\text{Hz}$  with  $21\text{kV}$  peak-to-peak, and (ii) sinusoidal voltage DBD at  $8.5\text{kHz}$  with  $16\text{kV}$  peak-to-peak. (This gap width is chosen as it is sufficiently large for the insertion of bacteria on the dielectric surface for sterilization application – to be discussed in Chapter 5.) The spectral emission from air-glass DBD and air-alumina DBD at sinusoidal voltage excitation is also compared. The tip of the fiber optic probe is held firmly with a retort stand and kept at constant distance of  $1.9\text{cm}$  away from plasma column (edge of the electrode).

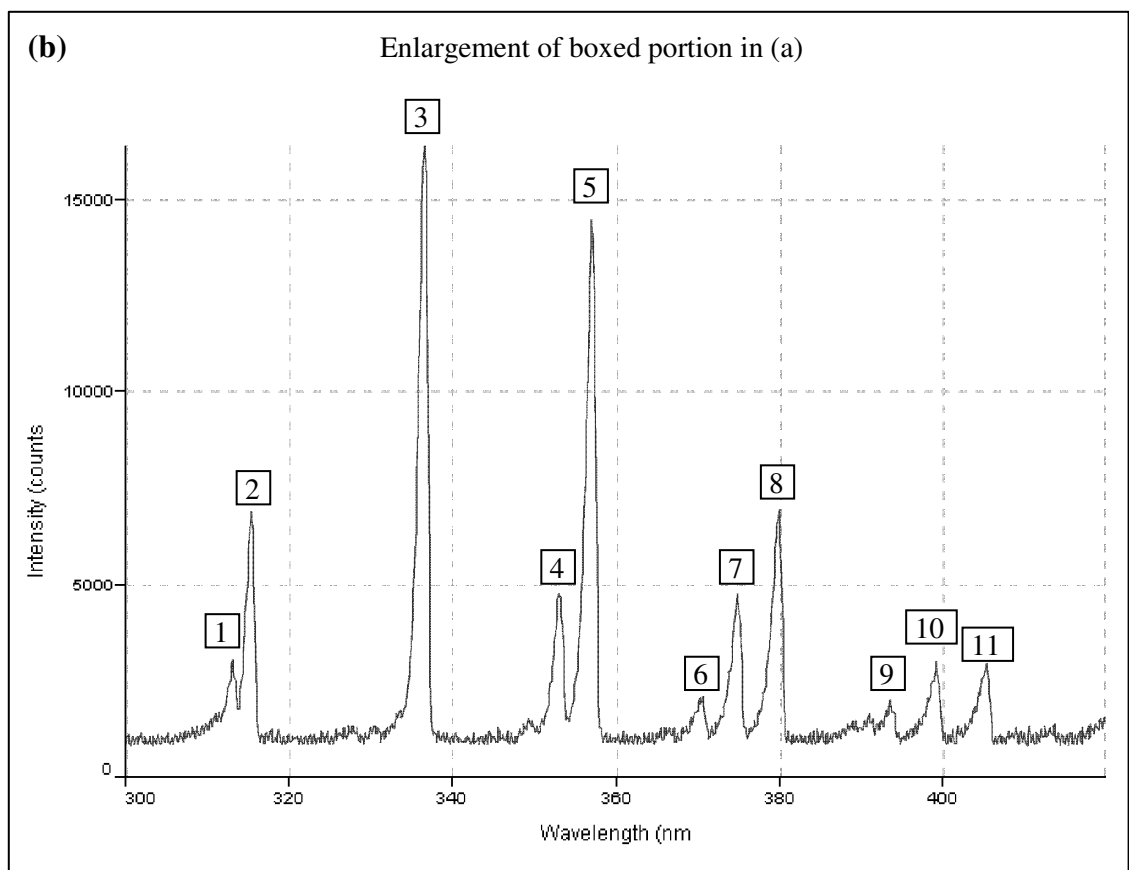
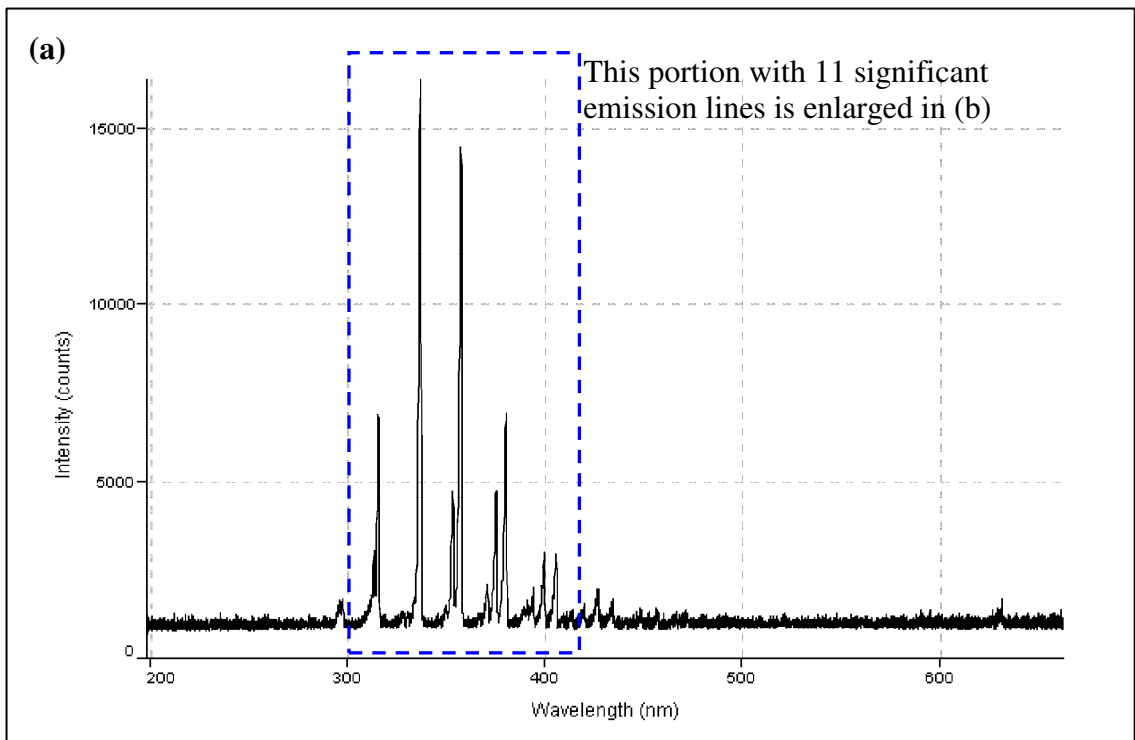


**Figure 4.30:** Typical emission spectrum from the 1.5mm air-gap DBD with glass barrier and sinusoidal voltage excitation; spectrometer set at 1s integration time.



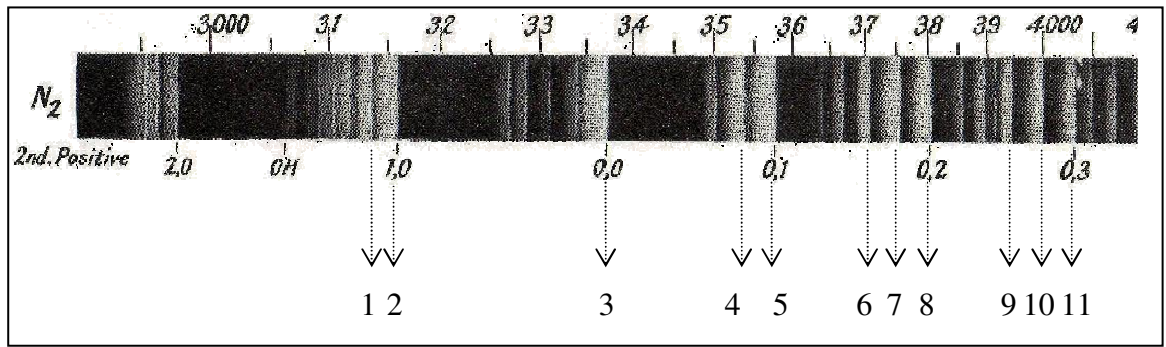


**Figure 4.31:** Spectrographic plate showing the second positive system,  $C^3\Pi_u - B^3\Pi_g$ , of molecular nitrogen from the positive column of discharge through  $N_2$  (Pearse and Gaydon, 1976). Numbers correspond to the emission lines in Figure 4.30(b).

From the optical emission spectra obtained, most of the strong emission lines fall between 300nm to 400nm. Typical spectrum from the air DBD (sinusoidal voltage excitation) with glass barrier is shown in Figure 4.30. By comparing the wavelength of the emission lines with standard spectroscopy database (Figure 4.31), the emission lines are found and identified as vibrational and rotational bands of the second positive system (SPS) of molecular nitrogen. The transition is between the  $C^3\Pi - B^3\Pi$  states of the neutral nitrogen molecule (Lofthus and Krupenie, 1977). This SPS spectra of the nitrogen has also been observed in a plasma pencil with flowing helium gas as reported by Laroussi and Lu, 2005, parallel-plate DBD with alumina barrier in air at 10Torr to 760Torr (Choi *et al.*, 2006), atmospheric pressure glow discharge (APGD) at 50Hz (Garamoon and El-zeer, 2009), and capillary DBD air plasma at 7kHz, 4kV rms (Mahoney *et al.*, 2010).

There are about eleven significantly strong SPS lines detected in this spectrum (Figure 4.30(b)), seven of which fall in the UV region and the remaining 4 lines in the VIS region. The UV emission line 3 has the strongest intensity compared to the others. The arbitrary intensity strengths (background spectrum deducted) for the identified emission lines are listed in Table 4.7. The lower intensity lines from the SPS spectra are

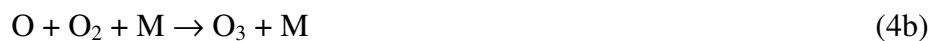


also identified and shown in Appendix B. Besides the spectra of the (i) SPS of N<sub>2</sub>, other lines identified include (ii) OH 306.4nm band, (iii) neutral oxygen atom lines (O I 595.84, 595.86, 625.68, 626.16nm – these lines register low intensity as the grating efficiency is below 40%), (iv) neutral molecular O<sub>2</sub> line (391.4nm), and (v) ionic molecular O<sub>2</sub><sup>+</sup> line (631.4nm). The presence of reactive species (e.g. OH, O) may be able to cause deactivation of bacteria.

Besides that, the existence of atomic oxygen, molecular oxygen and SPS of molecular N<sub>2</sub> spectra implies the possibility of production of ozone which is also a sterilization agent (Kim *et al.*, 1980). From qualitative observation, when the DBD is turned on, there is a distinct sharp odour which is peculiar to ozone (as low as 0.01ppm of ozone in air can be detected by most people through this distinct odour (Ozone, 2011)). Ozone may be produced through the process of electron impact collision (Eliasson *et al.*, 1987) as



followed by a three body collision,



where the third particle M can be O, O<sub>2</sub>, or O<sub>3</sub>. Another series of reaction involving the SPS of N<sub>2</sub> can produce oxygen atoms (Ahn *et al.*, 2003) leading to formation of ozone is given below.





For the determination of suitable DBD operation for bacteria inactivation, the emission spectra of strong lines from the DBD of “unipolar” pulsed and sinusoidal voltage excitation are compared (Figure 4.32) for glass barrier. Though both types of voltage excitation DBD exhibit identical emission spectra; the intensity of the emission spectrum from the sinusoidal voltage DBD is higher by 4-6 times (ratio G1/G2 in Table 4.7). It is deduced that the population of excited molecular nitrogen is greater in the sinusoidal voltage DBD. With reference to Figure 4.24, this is consistent with the much higher microdischarge density for the sinusoidal voltage DBD.

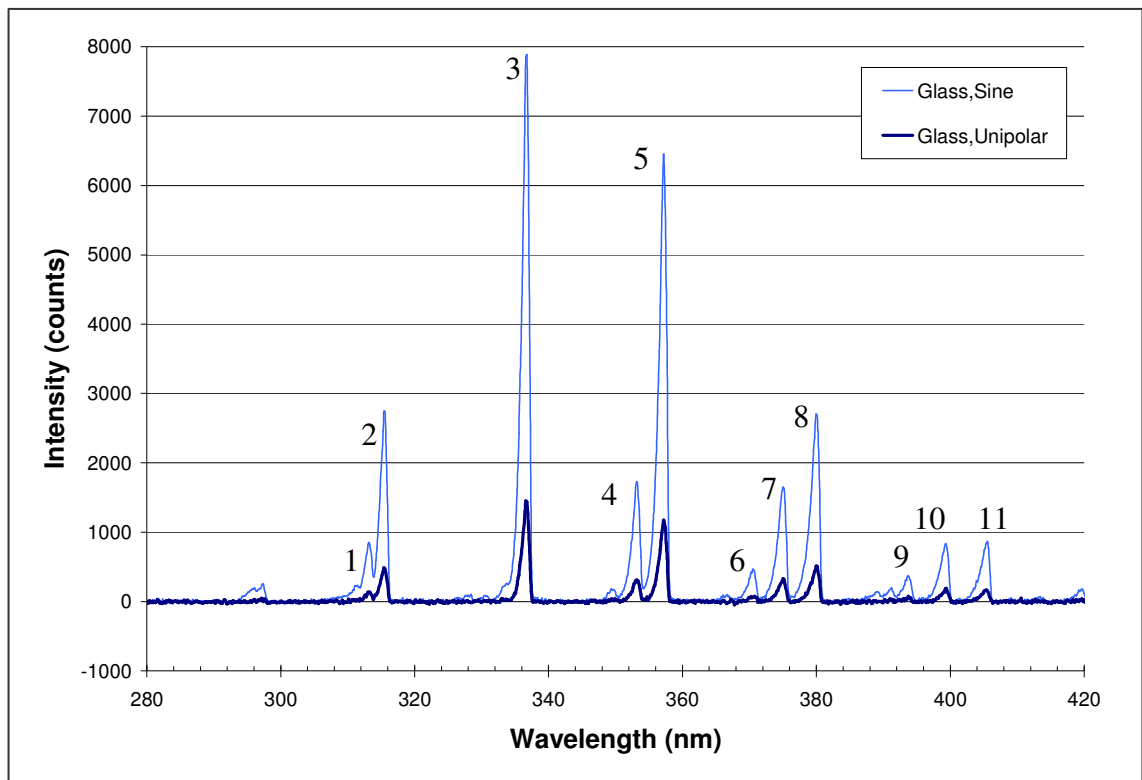


**Figure 4.32:** Overlay spectra from “unipolar” pulsed and sinusoidal voltage DBD with glass barrier. The spectra are recorded with 0.5s integration time with the background spectra deducted.

**Table 4.7:** Comparing the ratios of emission intensity (background deducted) of the identified emission lines from the stated DBD (sinusoidal voltage or “unipolar” pulsed excitation and glass or alumina barrier).

Line	Recorded Wavelength, nm ( $\pm 0.5$ nm)	Wavelength, nm (Pearse & Gaydon, 1976)	Intensity (Counts)				Ratios			
			GLASS barrier		ALUMINA barrier		G1/G2	A1/A2	A1/G1	A2/G2
			G1. Sinusoidal voltage DBD	G2. “unipolar” pulsed DBD	A1. Sinusoidal voltage DBD	A2. “unipolar” pulsed DBD				
1	313.1	313.60	851	137	838	187	6.2	4.5	1.0	1.4
2	315.4	315.93	2745	487	2456	655	5.6	3.7	0.9	1.3
3	336.7	337.13	7881	1451	7044	1955	5.4	3.6	0.9	1.3
4	353.1	353.67	1731	314	1535	434	5.5	3.5	0.9	1.4
5	357.2	357.69	6456	1176	5637	1563	5.5	3.6	0.9	1.3
6	370.6	371.05	465	76	452	102	6.1	4.4	1.0	1.3
7	375.0	375.54	1651	330	1503	409	5.0	3.7	0.9	1.2
8	380.0	380.49	2701	512	2414	685	5.3	3.5	0.9	1.3
9	393.7	394.30	370	79	340	97	4.7	3.5	0.9	1.2
10	399.4	399.84	830	192	750	203	4.3	3.7	0.9	1.1
11	405.5	405.94	866	167	756	206	5.2	3.7	0.9	1.2

Similarly in the case for alumina barrier, the emission intensities from sinusoidal voltage DBD is 3.5 to 4.5 times higher than that from “unipolar” pulsed DBD (ratio A1/A2 in Table 4.7). Next, the optical emission intensity from DBD with alumina barrier is compared to DBD with glass barrier (Figure 4.33) for sinusoidal voltage excitation. Though DBD with glass barrier exhibits higher intensity level, they are comparable (ratio A1/G1  $\approx$  1 in Table 4.7). This is inconsistent with the higher microdischarge density (almost doubled) recorded for alumina barrier in Figure 4.24. Referring to the physical appearance in Figure 4.28, it is probably because the filaments in alumina DBD seem to be denser at the center, implying that the light source is now further away from the fibre tip, hence, lower intensity level is recorded. Comparing the “unipolar” pulsed excitation for alumina and glass barriers (ratio A2/G2 in Table 4.7), alumina barrier records comparable though slightly higher intensity.

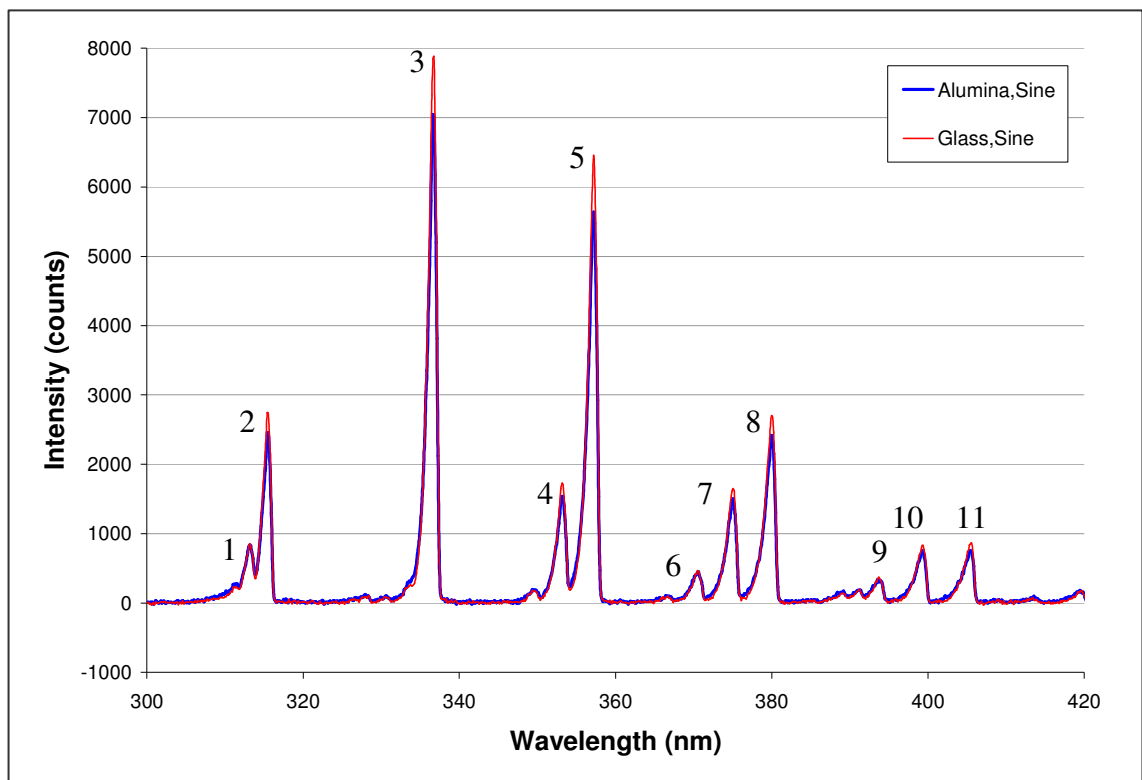


**Figure 4.33:** Overlay spectra from sinusoidal voltage DBD with glass barrier and alumina barrier. The spectra are recorded with 0.5s integration time.

## 4.4 Summary

The electrical characteristics of the DBD are summarized below:

1. The air-gap irrespective of type of dielectric barrier breaks down at electric field between 3kV/mm to 4kV/mm.
2. Series capacitance of the DBD (air-gap plus dielectric) has influence on the capacitive voltage and current profile of the discharge. With fixed MOSFET driving power ( $V_{DD}$ ), narrower air-gap increases the series capacitance resulting in decrease in resonance frequency of DBD system.
3. From the peak power calculated, “unipolar” pulsed DBD records higher value than the sinusoidal voltage DBD.
4. Current spikes (microdischarges) of FWHM 20ns are recorded on the rising and falling edges of both the “unipolar” pulsed and sinusoidal voltages, positive spikes at the rising edge while negative spikes at the falling edge. The sinusoidal voltage air-alumina DBD with 0.5mm air gap supports the highest number of current spikes. The number falls as the air gap increases and when voltage excitation is switched to “unipolar” pulsed type.
5. Dielectric material is critical in determining the charge deposition behavior. Alumina barrier with higher dielectric constant (9.0) produces discharge with more microdischarges as compared to glass barrier (7.5).
6. However, alumina barrier DBD seems to be more filamentary in appearance than glass barrier DBD. (The intense and well-defined filaments recorded over time scale of 1s implies many microdischarges forming at old site due to memory effect.) “Unipolar” pulsed DBD operation appears more diffuse (microdischarges are less likely forming at old sites) than sinusoidal voltage DBD.

7. From the optical emission spectra recorded for 1.5mm air gap, the sinusoidal voltage DBD with glass barrier records the highest intensity levels of the UV lines within the range of 300-400nm. Majority of the lines identified belong to the SPS of N<sub>2</sub> molecule. Other emission lines observed are probably from O, OH, O<sub>2</sub> and O<sub>2</sub><sup>+</sup>. Existence of SPS of N<sub>2</sub> molecule and atomic O spectra implies the possible formation of ozone.

The following DBD configuration is chosen to be applied for bacteria inactivation:

- i. “Unipolar” pulsed (500Hz) and sinusoidal voltage (8.5kHz) excitation for comparison purpose though sinusoidal voltage DBD exhibits lower peak power which can reduce thermal heating of specimen.
- ii. Glass barrier is used primarily it is readily available and cheap. Besides, it supports more diffused plasma as strong filaments can incur unwanted localized thermal heating. Furthermore, the sinusoidal voltage DBD with glass barrier has shown to emit the highest UV light
- iii. Though 0.5mm air gap produced the most diffused plasma, it is too narrow to insert the bacteria sample to be treated. Therefore, 1.5mm air gap is used. The 3.0mm air gap is unsuitable as the discharge is intermittently ignited at 8.5 kHz operation with strong filaments and it requires >10kV peak voltage to ignite.